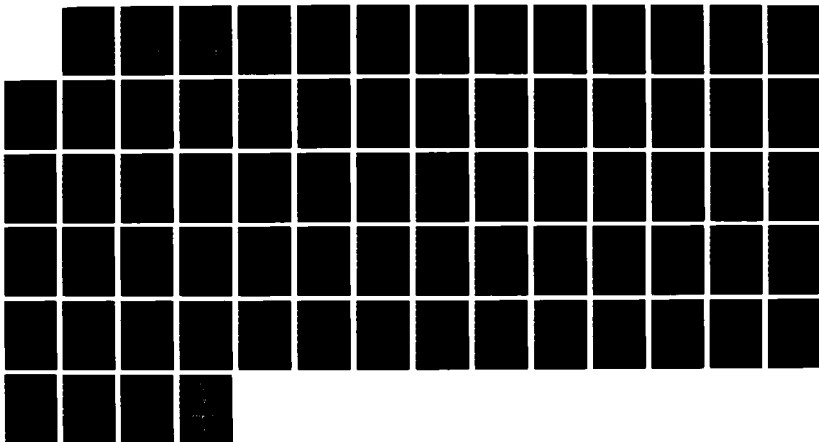
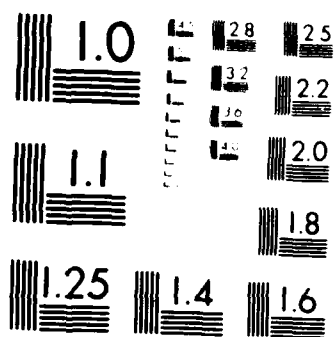


AD-A188 822

VALIDATION OF GENACS (GENERAL ELECTROMAGNETIC MODEL FOR THE ANALYSIS OF C. (U) AIR FORCE INST OF TECH 1/1  
WRIGHT-PATTERSON AFB OH SCHOOL OF ENGI.. D S HADDEE  
DEC 87 AFIT/GE/ENG/87D-39 F/G 20/3 NL

UNCLASSIFIED





MICROCOPY RESOLUTION TEST CHART  
 NATIONAL BUREAU OF STANDARDS-1963-A

AD-A188 822



DTIC FILE COPY

DTIC  
ELECTE  
FEB 09 1988  
S H D

VALIDATION OF GEMACS FOR MODELING  
LIGHTNING-INDUCED ELECTROMAGNETIC FIELDS

THESIS

David S. Mabee  
Captain, USAF

AFIT/GE/ENG/87D-39



DEPARTMENT OF THE AIR FORCE  
AIR UNIVERSITY  
**AIR FORCE INSTITUTE OF TECHNOLOGY**

Wright-Patterson Air Force Base, Ohio

**DISTRIBUTION STATEMENT A**

Approved for public release;  
Distribution Unlimited

88 2 4 0 6 2

AFIT/GE/ENG/87D-39

VALIDATION OF GEMACS FOR MODELING  
LIGHTNING-INDUCED ELECTROMAGNETIC FIELDS  
THESIS

David S. Mabee  
Captain, USAF

AFIT/GE/ENG/87D-39

DTIC  
ELECTE  
FEB 09 1988  
S H D

Approved for public release; distribution unlimited

VALIDATION OF GEMACS FOR MODELING  
LIGHTNING-INDUCED  
ELECTROMAGNETIC FIELDS

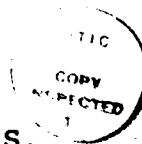
THESIS

Presented to the Faculty of the School Engineering  
of the Air Force Institute of Technology  
Air University  
In Partial Fulfillment of the  
Requirements for the Degree of  
Master of Science in Electrical Engineering

David S. Mabee, B.S.

Captain, USAF

December 1987



Acquisition For	<input checked="checked" type="checkbox"/>
NTIS	<input type="checkbox"/>
AD	<input type="checkbox"/>
DA	<input type="checkbox"/>
DTIC	<input type="checkbox"/>
DTIC/	<input type="checkbox"/>
ADDITIONAL	<input type="checkbox"/>
40811	<input type="checkbox"/>
DIST	<input type="checkbox"/>
Special	<input type="checkbox"/>
A-1	<input type="checkbox"/>

Approved for public release; distribution unlimited

## Acknowledgments

This thesis could not have been completed without help from others. First, I am very grateful to my faculty advisor, CPT Randy J. Jost, for his guidance and patience throughout the entire effort. MAJ Steve Woffinden, from Computer Science, and Dr. Alan Lair from Mathematics were my readers and provided much help in working the bugs out of the final document. I would also like to thank CPT Mary P. Hebert and CPT James Hebert, both formerly of AFWAL/FIESL, for their expert advice. Also, LT Rudy Braza provided great help in obtaining much of the data used in this thesis even while working on his own. Thanks to him for putting up with my requests when he undoubtedly had other things to do. Lastly, I could never have finished this thesis without the love and great patience of my wife Laura.

David S. Mabee

## Table of Contents

	Page
Acknowledgements . . . . .	ii
List of Figures . . . . .	v
Abstract . . . . .	vi
I. Introduction . . . . .	1
Overview . . . . .	1
Problem . . . . .	1
Background . . . . .	2
Objective of Research . . . . .	6
Approach . . . . .	6
Equipment/Materials Required . . . . .	7
Scope . . . . .	7
Assumptions . . . . .	7
Sequence of Presentation . . . . .	8
II. Theory . . . . .	9
Overview . . . . .	9
The Lightning Test Object . . . . .	9
Determining the Magnetic Fields . . . . .	11
III. Experiment . . . . .	17
Overview . . . . .	17
Experimental Setup . . . . .	17
Equipment . . . . .	18
Procedure . . . . .	19
Excitation Modeling . . . . .	22
IV. Modeling . . . . .	24
Overview . . . . .	24
GEMACS Electric Field Predictions . . . . .	24
GEMACS Files . . . . .	27
Geometric Modeling Considerations . . . . .	29
GEMACS Program Modules . . . . .	30
GEMACS Output . . . . .	31
V. Results . . . . .	33
Overview . . . . .	33
LTO Areas Analyzed . . . . .	33
Experimental Results . . . . .	35
GEMACS Results . . . . .	35

	Page
Comparison of GEMACS and Experimental Data . .	43
Summary of Results . . . . .	47
VI. Summary and Conclusions . . . . .	49
Overview . . . . .	49
Objectives Revisited . . . . .	49
Summary of Conclusions . . . . .	50
Recommendations . . . . .	50
Conclusion . . . . .	51
Appendix: GEMACS Files . . . . .	52
Bibliography . . . . .	58
VITA . . . . .	61



## List of Figures

Figure	Page
1. LTO/Return Path Setup . . . . .	10
2. Dimensions and TEM Field Configuration Around LTO . . . . .	12
3. Coordinate System Used in Modeling LTO . . . . .	12
4. Experimental Setup . . . . .	20
5. SFCW Input Current . . . . .	23
6. Integrated Sensor Response . . . . .	23
7. Frequency Domain Transfer Function . . . . .	23
8. Wire Grid Model of LTO . . . . .	28
9. Sensor Locations . . . . .	34
10. Experimental Transfer Function for LTO/Return Path . . . . .	36
11. Experimental Transfer Function for LTO . . . . .	37
12. Experimental Transfer Function for Return Path . . . . .	38
13. GEMACS Predicted Transfer Function for LTO/Return Path . . . . .	40
14. GEMACS Predicted Transfer Function for LTO . . . . .	41
15. GEMACS Predicted Transfer Function for Return Path . . . . .	42
16. Comparison of LTO/Return Path Transfer Functions. . . . .	44
17. Comparison of LTO Transfer Functions . . . . .	45
18. Comparison of Return Path Transfer Functions . . . . .	46
19. GIP Commands and Data for LTO . . . . .	54

Abstract

The "General Electromagnetic Model for the Analysis of Complex Systems" (GEMACS) is used to model and perform a frequency domain analysis on a specially instrumented Air Force Lightning Test Object (LTO). The predicted GEMACS results are compared to experimental data to evaluate GEMACS's ability to predict electromagnetic (EM) fields around the LTO. A previous elementary GEMACS study modeled an airplane and compared the results to lightning data collected inflight. Limitations of that effort included geometric modeling where some parts of the airplane were modeled more accurately than others and limited analysis bandwidth. The small bandwidth used in that GEMACS analysis made comparisons (with the inflight data) difficult because the inflight data had a much larger bandwidth. The present study analytically models the LTO most accurately at the places where field predictions are made and uses a larger analysis bandwidth of 1 - 100 MHz. This study provides an enhanced baseline case on how accurately GEMACS predicts lightning induced EM fields, and further validation that frequency domain code analysis can provide an economical method by which lightning's interaction with aircraft can be predicted.

# VALIDATION OF GEMACS AS A MODEL FOR LIGHTNING-INDUCED ELECTROMAGNETIC FIELDS

## I. Introduction

### Overview

This thesis assesses the accuracy of the Air Force's General Electromagnetic Model for the Analysis of Complex Systems (GEMACS) to predict lightning-induced electromagnetic (EM) fields around a specially instrumented Lightning Test Object (LTO). For the GEMACS analysis, the LTO was analytically modeled and injected with representative currents at lightning frequencies. GEMACS calculated the electric fields at a point on the LTO. The predicted electric fields were converted to magnetic fields and compared to measured data to determine how accurately GEMACS predicted lightning-induced EM fields.

### Problem

This thesis used GEMACS to predict lightning-induced EM fields around the LTO. The results of the GEMACS analysis were compared to data measured on the LTO during actual current injection tests to determine how accurately GEMACS modeled lightning-induced EM fields.

## Background

Lightning. According to Uman, "A lightning strike is a transient, high current, electric discharge whose path length is generally measured in kilometers" (22:1).

"Cumulonimbus clouds produce most lightning events" (22:1).

Lightning may occur within a cloud (intra-cloud lightning), between clouds (inter-cloud lightning), between cloud and ground (cloud-to-ground lightning), and between a cloud and surrounding air (air discharges) (22:1,2).

Lightning occurs because of charge separation and the subsequent creation of positive and negative charge centers. In the case of cloud-to-ground lightning, the cloud and ground are the charge centers. The cloud is usually the negative charge center and the ground the positive although the opposite is sometimes true. In this report only the more common negative cloud, positive ground case will be considered. When the potential between the charge centers becomes too great for the atmosphere to support, a weakly luminous negative predischage propagates from the cloud towards the ground in a stepped fashion. This is called the "stepped leader" process. When the stepped leader is approximately 100-200 feet from the ground, a leader of opposite polarity forms and moves up from the ground towards the stepped leader tip. When the two meet, the stepped leader channel is lowered to ground potential by the return stroke. The return stroke propagates from ground-to-cloud through the channel created by the stepped leader and is the highly luminous "streak-of-lightning" seen during

thunderstorms. A typical return stroke carries peak currents of 20 kiloamperes (kA). The maximum rate-of-change of the return stroke can be higher than 15 kA/microsecond. The return stroke energy heats the lightning channel to temperatures nearing 30,000 degrees Kelvin generating a high pressure channel which expands faster than the speed of sound thereby creating the characteristic thunderclap (22:5-9).

Lightning and Aircraft. Aircraft caught between the charge centers can become part of the lightning channel (20:3-5). "When lightning strikes an aircraft, the damage occurring is generally of two basic types." The first type is physical damage resulting from a direct attachment (8:2). This sort of damage is characterized by pitting, burning, blasting, etc. on the aircraft skin and is called "direct effects" damage (8:2). Newer aircraft, which make use of nonconductive composite and fiberglass materials, are much more susceptible to this type of damage than older aluminum and titanium aircraft (3:1). Since lightning usually attaches at one of the extremities, direct effects damage is usually seen at pitot booms, radomes, wing tips, and antennas. The other type of damage results from the quickly changing EM fields caused by currents flowing on the aircraft skin when it is struck by lightning. Nearby lightning and nuclear EM pulse (NEMP) also produce EM fields which intercept the aircraft. These fields can couple into the interior of the aircraft via joints, antennas, cracks,

and apertures on the aircraft skin. The fields can then induce voltage and current transients in the internal wiring and subsequently in the avionics. The high levels and/or rate of change of these voltage/current transients may be enough to upset or cause damage to newer generation avionics systems which operate on lower power levels than earlier avionics (8:2).

Recent Lightning Research. The use of composite materials and low power electronics in advanced technology aircraft has sparked a renewed interest in the lightning/aircraft interaction event. Rustan noted:

In the past ten years, at least five different aircraft have been instrumented and flown in and around thunderstorms to measure the EM characteristics of lightning discharge. This work was done to identify the expected lightning threat environment to a flying aircraft (20:2).

From this research, engineers in the U.S., Great Britain, and France have been able perform realistic simulation and modeling experiments because they have known what current levels and waveforms are experienced by an aircraft that has been struck by lightning.

In the U.S., the Air Force Wright Aeronautical Laboratory (AFWAL) has carried out lightning simulation experiments, either in-house or through contract, on the F-14, All-Composite Airframe Program (ACAP), CV-580, Lightning Test Object (LTO) and various other testbeds (1,10,18). The British have performed simulation on their

Hawker Hunter lightning test rig, Jaguar fighter, and Lynx helicopter (2,4,9). French lightning simulations have been carried out with their test cylinder (15).

In the area of computer modeling, all three countries have developed programs for analyzing lightning/aircraft interactions. AFWAL has shown GEMACS to be a powerful tool in predicting lightning-induced aircraft skin current distributions (5,20). GEMACS incorporates either Method of Moments (MOM), Geometrical Theory of Diffraction (GTD), or a hybrid MOM/GTD solution technique (13:3).

In a previous study, a GEMACS analysis was performed on a CV-580 aircraft (21). The GEMACS results were compared to lightning data collected by the CV-580 inflight. The GEMACS analysis missed several resonances indicated in the inflight data. These differences were attributed to the complex geometry of the aircraft and the limited bandwidth used in the GEMACS analysis. These reasons led to this follow on study using a more simple structure, the LTO, and a larger analysis bandwidth.

The British have developed two programs, INDCAL and POTENT, for use in lightning analysis. These programs use a two-dimensional finite-difference solution technique to solve Maxwell's equations for the surface currents on an aircraft. INDCAL and POTENT have shown excellent agreement with measurements made on the Culham Hawker Hunter test rig (3:6).

The French have concentrated their efforts on a three-dimensional finite-difference (3DFD) surface current solution technique and have obtained good agreement with their measured results though at the cost of long computer runtimes (11). This technique is similar to that used by Williford to model interactions with a CV-580 aircraft (23). In that analysis, good agreement was reached with airborne strike data but again at considerable cost in terms of mainframe CPU times.

#### Objective of Research

The objective of this thesis was to validate the program GEMACS for predicting lightning-induced EM fields by comparing its predictions with measured data.

#### Approach

The major tasks involved in this effort were:

- a. Construct a wire grid model of the LTO  
in accordance with the GEMACS Engineering and User manuals (12,13).
- b. Perform the GEMACS analysis to predict the electric fields around the LTO.
- c. Deduce magnetic field predictions from the electric field predictions.
- d. Compare the GEMACS predictions to measured data to assess the accuracy of the model.



The results of this analysis are graphs comparing GEMACS predicted fields to measured data.

#### Equipment/Materials Required

The measured lightning data came from research performed at the Air Force Wright Aeronautical Laboratories lightning simulation facility. The GEMACS program is installed and resident on a VAX 11/785 computer at AFIT.

#### Scope

The following is a summary of the limitations of this study:

- a. This thesis considered only the problem of external EM fields. It did not address the lightning attachment process, the external to internal coupling of EM fields or the coupling of fields into internal wiring.
- b. Only the nose-entering/tail-exiting strike was investigated because it is considered the most typical (18:7).

#### Assumptions

One general assumption made for this study was that the small discontinuities on the LTO such as weld marks and small cracks could be neglected when making measurements and predictions. This assumption can be made because the discontinuities are small as compared to the wavelength of

the lightning currents (19:16). Another assumption was that the nonlinear effects of corona and electrical breakdown in gases could be neglected because they tend to decrease the magnitude of the lightning energy threat.

#### Sequence of Presentation

Chapter II overviews the transmission line theory used to predict the magnetic fields. Chapter III describes the experimental analysis of the LTO. Chapter IV describes the GEMACS analysis process. Chapter V presents the results of the GEMACS and experimental measurements and compares the two. Chapter VI summarizes the effort and makes recommendations for future research efforts.

## II. Theory

### Overview

This chapter gives an explanation of the EM theory used to predict magnetic fields around the LTO. GEMACS is used to calculate electric fields around the LTO when injected with lightning frequency currents. Then, using transmission line theory, magnetic fields were predicted using the electric field calculations.

### The Lightning Test Object

The LTO was the test bed used for this thesis. Designed to model the fuselage of an aircraft, the LTO is a cylinder with conical end caps. The LTO is over ten meters long with a diameter of about one meter. A coaxial return path was placed around the LTO for the Swept Frequency Continuous Wave (SFCW) and Current Pulse tests. A picture of the LTO/return path setup is given in Figure 1. The return path was designed to provide a uniform EM field distribution around the cylinder and gives the entire setup the appearance and physical characteristics of a coaxial transmission line. For this reason coaxial transmission line theory can be used next to predict the magnetic fields around the cylinder if the electric fields are known.

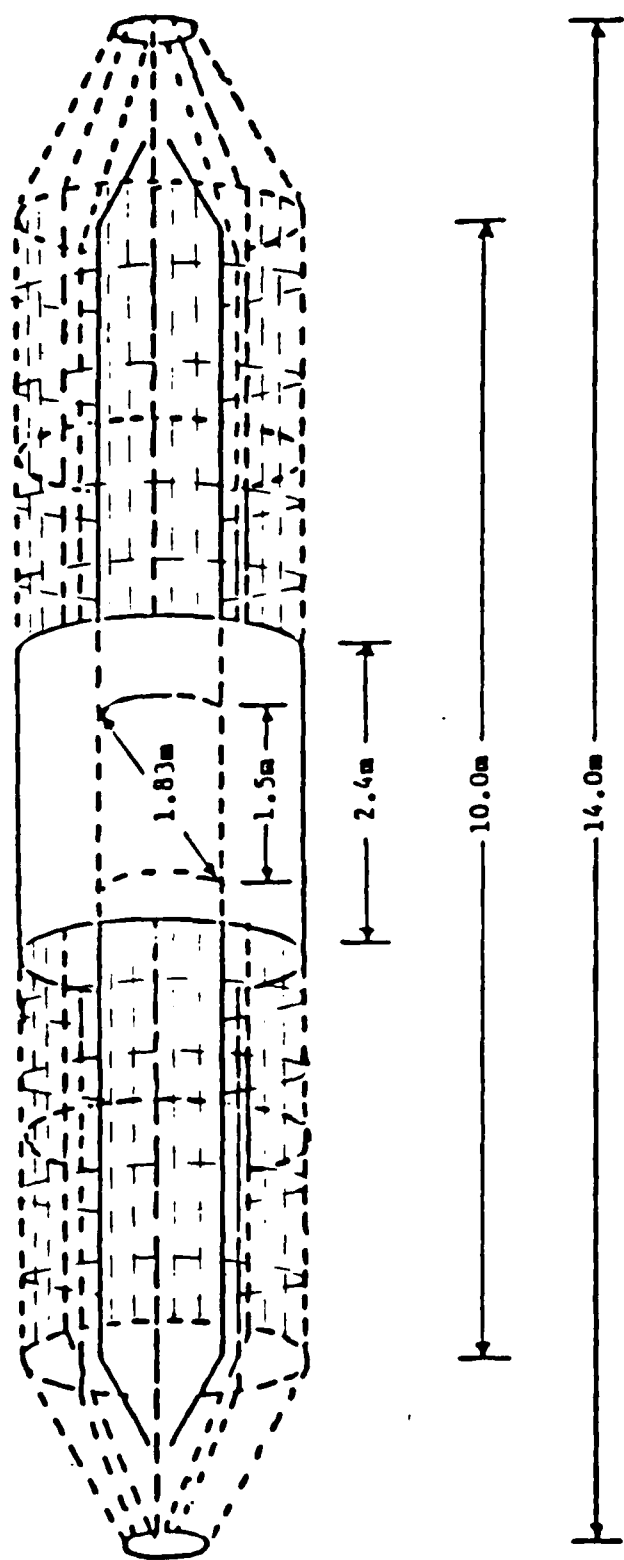


Figure 1. LTO/Return Path Setup

### Determining the Magnetic Fields

Since only magnetic fields were measured on the LTO, a method of converting GEMACS's electric field predictions to magnetic field predictions had to be found. To calculate these magnetic fields an algorithm was developed. First, the LTO/return path combination was assumed to be a lossless coaxial transmission line with cross sectional dimensions as shown in Figure 2. When current is injected down the center conductor of the coaxial transmission line formed by the LTO and return path, the magnetic field lines are considered to be concentric circles about the LTO and the electric field lines are radial as shown in Figure 2 (14:367). This field configuration is called a Transverse Electro Magnetic (TEM) field because the electric and magnetic fields are entirely transverse to the direction of propagation. This is the only field configuration possible under steady state conditions or for time-varying situations when the wavelength is of the order four times the outer radius or greater (14:367). As the wavelength approaches the transverse dimensions of the transmission line, more complex field configurations known as higher order modes can exist in which fields have components in the axial direction (14:367,368).

A TEM wave will be assumed to flow on the LTO with propagation in the -x direction. Maxwell's equations for a lossless, isotropic and homogenous medium between the outer and inner conductors are given by:

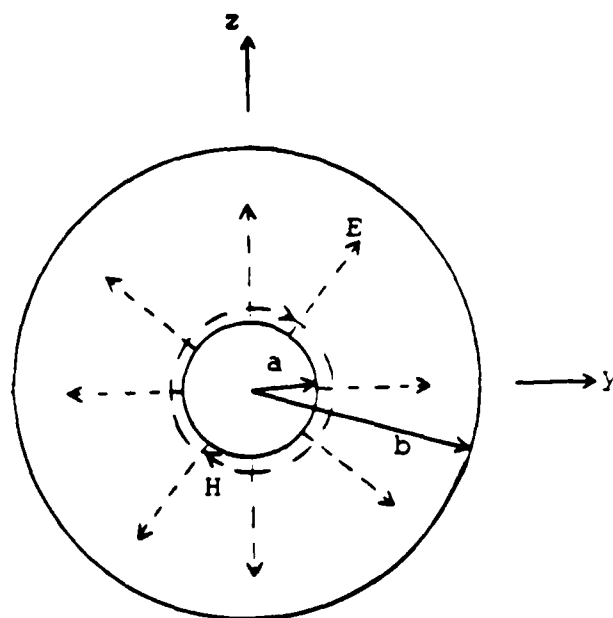


Figure 2. Dimensions and TEM Field Configuration Around LTO

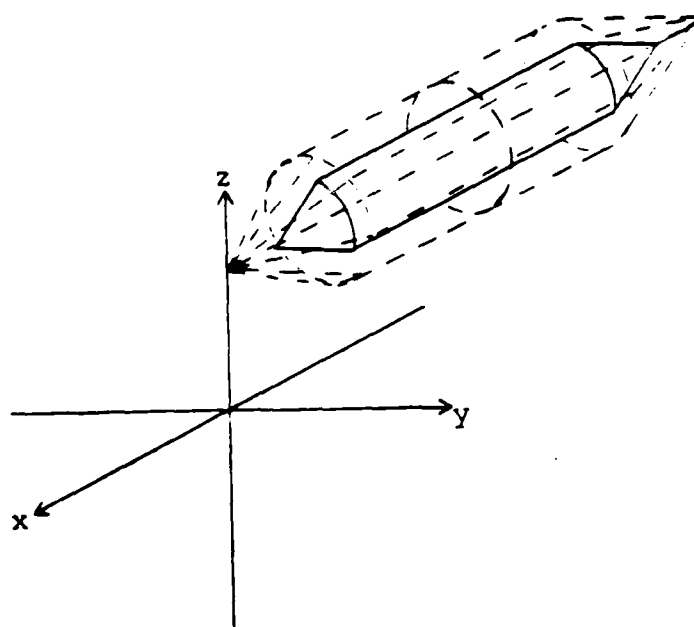


Figure 3. Coordinate System Used in Modeling LTO

$$\nabla \times E_t = -j\omega u H_t \quad (1)$$

$$\nabla \times H_t = j\omega e E_t \quad (2)$$

where

H = magnetic field intensity [A/m]  
 E = electric field intensity [V/m]  
 $\omega$  = angular frequency [radians/sec]  
 u = magnetic permeability [H/m]  
 e = electric permittivity [F/m]  
 $\nabla \times$  = curl operator

and the subscript t indicates that the fields have components in the transverse (y and z) directions only.

The vector operator  $\nabla$  may be separated into transverse and longitudinal components:

$$\nabla_t = a_y \frac{\partial}{\partial y} + a_z \frac{\partial}{\partial z} \quad (3)$$

$$\nabla_x = a_x \frac{\partial}{\partial x} \quad (4)$$

$\nabla_t \times E_t$  and  $\nabla_t \times H_t$  are vectors orthogonal to the transverse plane. Since the fields are considered purely transverse, equations (1) and (2) reduce to:

$$a_x \times \frac{\partial E_t}{\partial x} = -j\omega u H_t \quad (5)$$

$$a_x \times \frac{\partial H_t}{\partial x} = j\omega e E_t \quad (6)$$

$$\nabla_t \times E_t = 0 \quad (7)$$

$$\nabla_t \times H_t = 0 \quad (8)$$

In vector fields, when the curl of a vector is zero, it may be obtained from the gradient of a suitable scalar function. Knowing this, equations (7) and (8) will be satisfied if:

$$E_t = g_1(x) \nabla_t \phi \quad (9)$$

$$H_t = g_2(x) \nabla_t \psi \quad (10)$$

where  $g_1$ ,  $g_2$ ,  $\phi$  and  $\psi$  are scalar functions to be determined.  $\phi$  and  $\psi$  are functions of the transverse coordinates  $y$  and  $z$  only, since it is only the transverse curl which vanishes. The form of solution given in (9) and (10) is possible because the vector Helmholtz equation in rectangular coordinates is separable. Since a source-free medium is being assumed, the divergence of the field vectors is zero. Equations (9) and (10) show that  $\phi$  and  $\psi$  are solutions of Laplace's equation in the transverse plane transverse plane; that is,  $\nabla_t^2 \phi = 0$ , and similarly for  $\psi$ . The scalar functions  $\phi$  and  $\psi$  are not independent since  $E_t$  and  $H_t$  are related by (5) and (6). Differentiating (5) with respect to  $x$  and substituting from (6) after cross-multiplying both equations by  $a_x$  gives:

$$a_x \times a_x \times \frac{\partial^2 E_t}{\partial x^2} - w^2 u e E_t = 0 \quad (11)$$



Rewriting this result gives:

$$\frac{\partial^2 E_t}{\partial x^2} + k^2 E_t = 0 \quad (12)$$

where  $k^2 = w^2 u e$ . The solution to (10) gives the function  $g_1(x)$  the form  $(A_{\pm}) \exp(\mp j k x)$ , where  $A_{\pm}$  are amplitudes. Since a function  $\exp(j \omega t)$  was assumed,  $A_{+} \exp(-j k x)$  represents propagation in the positive  $x$  direction and  $A_{-} \exp(j k x)$  represents propagation in the negative  $x$  direction. The propagation constant  $k$  is given by:

$$w(u e)^{1/2} = \frac{w}{c} = \frac{2 \pi f}{c} = \frac{2 \pi}{\lambda} \quad (13)$$

where  $c$  is the velocity of light in a medium with parameters  $u$ ,  $e$  and  $\lambda$  is the wavelength corresponding to frequency  $f$  in the same medium. The solution for the electric field can be written as:

$$E_t = (A_{\pm}) \nabla_t \phi(y, z) \exp(\mp j k z) \quad (14)$$

The solution for the magnetic field can be found from (3) as:

$$H_t = \pm \left( \frac{e}{u} \right)^{1/2} a_x \times \nabla_t \phi (A_{\pm}) \exp(\mp j k x) \quad (15)$$

Substituting from equation (12) into (13) yields:

$$H_t = \pm \left( \frac{e}{u} \right)^{1/2} a_x \times E_t \quad (16)$$

The factor  $(u/e)^{1/2}$  has the dimensions of ohms and is called the intrinsic impedance of the medium (6:67-69). For an air-filled transmission line:

$$\left(\frac{u}{e}\right)^{1/2} = \left(\frac{u_0}{e_0}\right)^{1/2} = 377 \text{ ohms} \quad (17)$$

(6:136).

Since the LTO is modeled as a lossless coaxial transmission line, the magnetic fields are directly proportional to the electric fields as long as the wavelength is sufficiently large compared to the dimensions of the line.

The theory discussed in this chapter allows the magnetic fields to be calculated if the electric fields are known and allows comparisons to be made between the GEMACS electric field predictions and experimentally measured magnetic field data. Equation (16) gives a direct relationship between the electric and magnetic fields in a coaxial transmission line. A description of the GEMACS analysis is given in chapter IV. The next chapter describes how the experimentally measured data was obtained.

### III. Experiment

#### Overview

This chapter describes the how the experimental data used in this thesis was collected. The LTO setup, equipment used to excite the LTO, and measurement and data processing equipment are discussed. During the time that this thesis was being performed, other related research efforts were being performed that provided much of the experimental results used in this study. Jost and Braza produced transfer functions of the LTO/return path combination and the separate components of the LTO set up including the return path alone and the cylinder alone.

#### Experimental Setup

The LTO. The LTO was designed by Hebert and constructed by AFIT for lightning coupling research. It was meant to model the fuselage of an aircraft so it was constructed of 0.06 inch thick sheet aluminum and assembled using aircraft construction techniques. The LTO is over ten meters in length and has a diameter of approximately one meter. The LTO was built with an aperture in the center in order to study the effects of aperture coupling and the EM shielding properties of different panels placed in the aperture. The aperture is 1.5 meters long and spans 120

degrees of the cross section of the cylinder. An aluminum panel was placed in the aperture for this thesis in order to closely approximate a perfect conductor.

The Return Path. A coaxial return path was placed around the LTO during the SFCW and Current Pulse tests. The return path provided a uniform EM field distribution around the LTO. The return path is approximately 14 meters long and has a diameter of just over 2 meters. The section of the return path over the aperture is made of sheet aluminum. The rest of the return path is made of wire mesh with the longitudinal wires spaced about every two degrees around the cylinder. In past experiments the longitudinal wires were spaced every twenty degrees. The more dense mesh was constructed so that the return path would approximate a solid surface at higher frequencies. Figure 1 shows the LTO/return path combination.

#### Equipment

Along with the LTO and coaxial return path were excitation, measurement and data processing equipment. A Hewlett-Packard 3577A network analyzer and power amplifier were used to excite the LTO and measure the sensors' responses. EG&G magnetic (B-dot) field sensors were used to measure the magnetic fields. A PDP 11/34 computer collected and processed the data.

## Procedure

The experimental measurements were made by Captain Randy J. Jost of AFIT/ENG. The LTO and return path were designed as a coaxial transmission line with a radius ratio of 2.3 to give a characteristic impedance of approximately 50 ohms. A matched load of 50 ohms is placed at the end of the LTO to reduce reflections as much as possible. A diagram of the experimental setup is shown in Figure 4. The set up and tests used to derive the transfer functions of the LTO are known as the Swept Frequency Continuous Wave (SFCW) test method. With this method of the network, the analyzer provides a CW signal which is swept from near DC to 100 MHz. The signal from the network analyzer is fed through a power amplifier to increase its strength to 25 watts. The amplified signal is then applied to the LTO and also fed back to the network analyzer. Figure 5 shows a time domain representation of the input SFCW current. The EG&G CML-7 B-dot sensor measures the magnetic field due to the SFCW current. The sensor response is fed into the network analyzer. The magnetic field sensor is a derivative sensor responding to the time rate of change of the corresponding magnetic field. The field sensor is a passive device, requiring no external power. The equation describing the response of the sensor is

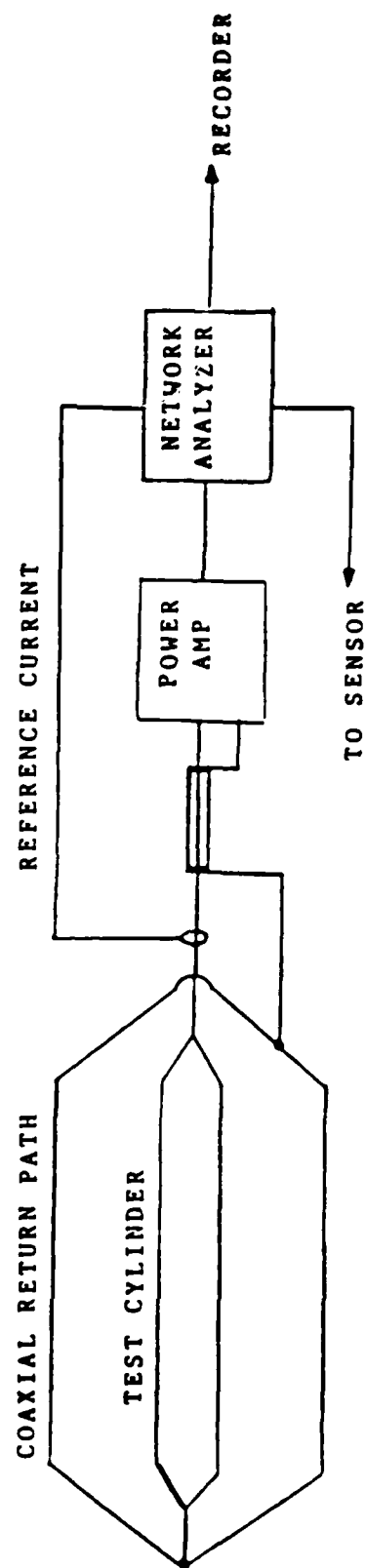


Figure 4. Experimental Setup

$$V_0 = A_{eq}(dB/dt) \quad (18)$$

where

$V_0$  = output voltage (volts)  
 $A_{eq}$  = sensor equivalent area (square meters)

$B$  = magnetic flux density vector (teslas)

The input waveform and sensor response waveforms are fed through fiber optic links to the PDP 11/34 computer and are stored on magnetic disks. The sensor response,  $dB/dt$ , is divided by  $u_0$  to obtain the derivative of the measured magnetic field,  $dH/dt$ . This term contains the effects of the measurement apparatus which need to be eliminated to obtain the actual magnetic field. A Fast Fourier Transform (FFT) is done on the  $dH/dt$  data to put it in the frequency domain. An FFT is also done on the derivative of the transfer function of the sensor. This derivative sensor transfer function, now in frequency domain, is divided into the measured magnetic field data. A natural integration takes place along with dividing out the effects of the measurement system, leaving only the actual magnetic field, the desired information. The magnetic field data is divided by the input current to obtain the magnetic field transfer function of the cylinder. Figures 6 and 7 show the integrated time domain sensor response (magnetic field) and frequency domain transfer function respectively.

### Excitation Modeling

In the experimental procedure, the LTO was excited by a swept frequency CW signal of constant amplitude. GEMACS provided only a delta-gap electric field method of exciting wires. But, since transfer functions were compared, the excitation method did not matter because the transfer function of a linear system is the same regardless of input (7:38,9). The GEMACS analysis was performed in the frequency range 1 - 100MHz while the experimental analysis was performed from 0.1 - 100MHz (10:5,6).



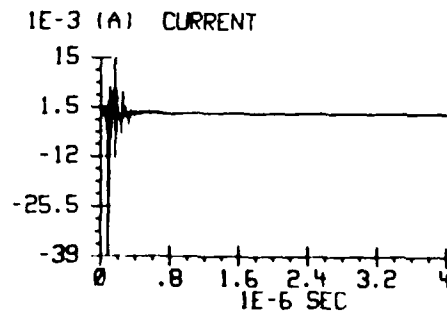


Figure 5. SFCW Input Current

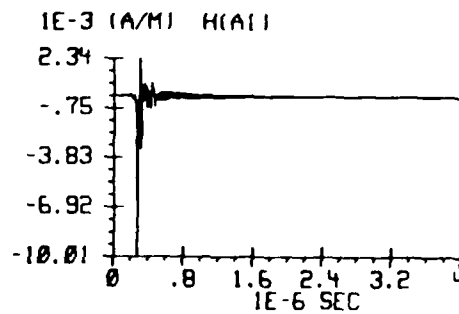


Figure 6. Integrated Sensor Response

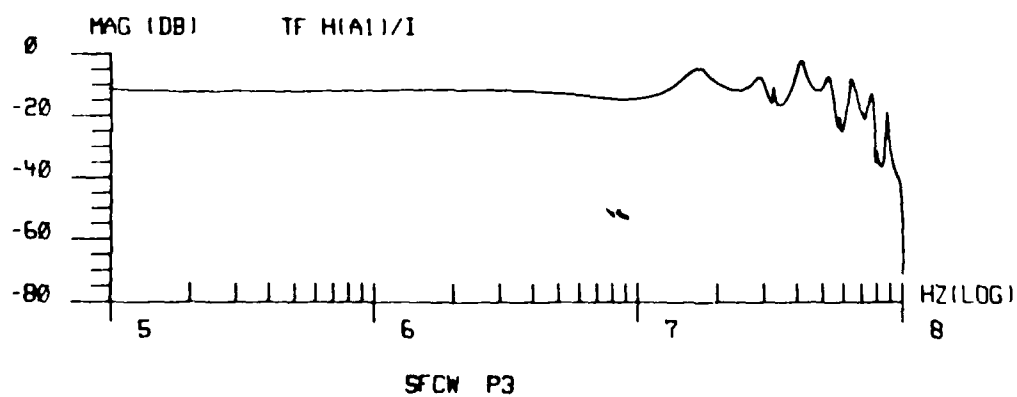


Figure 7. Frequency Domain Transfer Function

## IV. Modeling

### Overview

This chapter reviews the GEMACS analysis that was performed to model and predict the EM events that occurred in the experimental measurements. The EM interactions are modeled in GEMACS using the Method of Moments (MOM) approximation to the solution of Maxwell's equations. For this analysis, a GEMACS geometry file is generated in which the LTO is modeled as a wire grid. The GEMACS executive program file is used to specify the analysis frequency, the method of solution (MOM), excitation of the structure and form of the output of data. The program file was then attached to the geometry file and executed using the GEMACS program modules. The output consisted of electric field predictions at specified points around the LTO.

### GEMACS Electric Field Predictions

EFIE and MFIE. GEMACS is a program which was developed by the Air Force that can be used to solve a wide variety of EM problems. Solutions predicted by GEMACS are based on the numerical solution of either the electric field integral equation (EFIE) or the magnetic field integral equation (MFIE) or both (13:3). The EFIE and MFIE are obtained by recasting Maxwell's differential equations (13:4):

$$\frac{\partial \bar{B}}{\partial t} = - \nabla \times \bar{E} \quad (19)$$

$$\frac{\partial \bar{D}}{\partial t} = \nabla \times \bar{H} - \sigma \bar{E} \quad (20) \quad \bar{D} = e \bar{E} \quad (23)$$

$$\nabla \cdot (\bar{D}) = p \quad (21) \quad \bar{B} = u \bar{H} \quad (24)$$

$$\nabla \cdot (\bar{B}) = 0 \quad (22)$$

where

$\bar{H}$  = magnetic flux density (amperes/meter)  
 $\bar{E}$  = electric field intensity (volts/meter)  
 $t$  = time  
 $u$  = magnetic permeability (Henries/meter)  
 $e$  = electric permittivity (Farads/meter)  
 $p$  = charge density (Coulombs/meter)  
 $\sigma$  = conductivity (mhos/meter)  
 $\nabla \times$  = vector curl operator  
 $\nabla \cdot$  = vector divergence operator

into an integral equation. The two most widely used integral equations are the EFIE and the MFIE (13:3):

$$\tau \cdot \bar{E}^i = \frac{j\omega u}{4\pi} \cdot \int_1 IG(\bar{r}, \bar{r}') d\bar{l} \quad (\text{EFIE})$$

$$\bar{n} \times \bar{H}^i =$$

$$\frac{1}{2} \bar{J}_s - \frac{1}{4\pi} \bar{n} \times \oint_s [\bar{J}_s \times \nabla G(\bar{r}, \bar{r}')] d\bar{s} \quad (\text{MFIE})$$

where

$G(\bar{r}, \bar{r}') = \exp(-jkr)/R$ ; free space Green's function  
 $\bar{r}'$  = distance from origin to observation point  
 $\bar{r}$  = distance from origin to source point  
 $R = |\bar{r} - \bar{r}'|$ ; distance from observation point to source point

Kadlec states:

"The EFIE expresses structure currents in terms of a Green's function and incident electric fields and is well suited to one-dimensional geometries such as thin wires or geometries composed of thin wires. The MFIE expresses surface currents in terms of the derivative of Green's function and incident magnetic fields and is well suited to smooth, closed surfaces" (13:3).

Method of Moments. One of the solution techniques offered by GEMACS for solving these integral equations is the Method of Moments (MOM). MOM relies on linearity and superposition. The MOM is called a subsectional method because it relies on reducing either or both of the integral equations into a set of linear simultaneous equations. This is normally done by modeling the structure through a set of basic objects such as thin wires or surface patches (13:6,7). "A conducting wire mesh will behave approximately as if it were a solid surface, provided that the mesh size is small compared with wavelength" (17:7).

Within the domain of each object, a current of known functional form but unknown amplitude is assumed as the solution of the integral equation. By linearity, the unknown current amplitude coefficients are factored out of the integral. Then, the integral can be solved either directly or numerically. The field at any point in space due to the current at any point on the structure is then specified and superposition can be used to compute the total field. For a perfectly conducting body, the best point at which to compute the total field is at the surface of the

structure because there it is known that the tangential electric and normal magnetic fields are identically zero.

The field distributions of each object are weighted to obtain a scalar field value associated with each object. The unknown current coefficients are then found by solving the resulting matrix problem. Then the current coefficients can be used to determine the current distributions over the entire structure (13:6,7).

The MOM can be particularly useful for lightning/aircraft interaction problems because it is a low frequency (dc - 100 MHz) technique. The frequency of lightning EM energy typically falls in the dc to 20 MHz range (21:15,16).

#### GEMACS Files

The LTO is modeled as a wire grid for this GEMACS analysis. The first step in this modeling process was to obtain a drawing of the LTO including its various dimensions. This was accomplished by actually measuring the LTO with a tape measure. A drawing of the LTO with all its pertinent dimensions is given in Figure 1. The next step in the modeling process is to make a wire grid model of the LTO from the drawing. The GEMACS Engineering and User manuals give guidelines to follow when dividing the drawing into segments. Tomko developed a step-by-step approach to constructing a wire grid model in his thesis (21:99-113). Figure 8 gives a wire grid representation in two views of

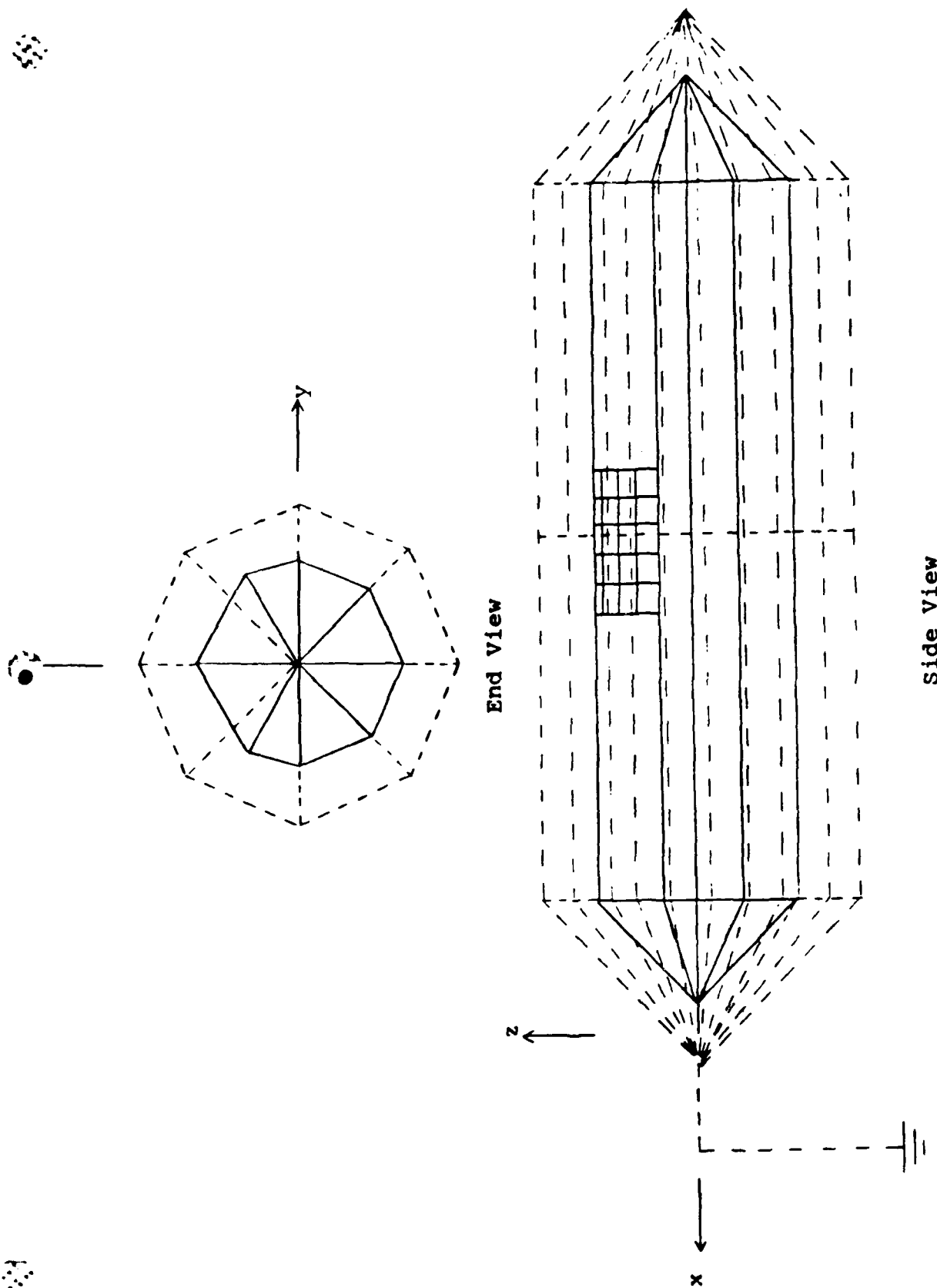


Figure 8. Wire Grid Model of LTO

the LTO. A description of the steps used to wire grid model the LTO is given in the Appendix along with a copy of the file containing the GEMACS geometry file.

The GEMACS program file is a set of instructions written to perform the analysis on the geometrical representation of the LTO. First, the program file sets the analysis frequency range, chooses the method of analysis (MOM) and inputs the excitation sources. Next, the program calculates the interaction matrix, performs the analysis and provides the electric field values as output.

#### Geometric Modeling Considerations

In the results section of this thesis, one way of comparing the experimental results to the predicted results will be to compare locations of resonances or peaks in the responses. Natural modes of resonance exist on the LTO/return path combination due to the dimensions of the set up. Natural resonances also exist due to the geometric dimensions of aircraft. It is at these resonant frequencies that the highest lightning threat occurs. On the LTO, for example, resonances could exist due to the lengths or diameters of the LTO or return path. At the lower frequencies, the entire set up will be smaller than a wavelength and the resulting current distribution will be essentially static. As the frequency increases, the lengths of the segments in the LTO wire grid model will become more comparable to a given wavelength and resonances could be

predicted where none are measured experimentally. For instance, in modeling the LTO and return path as a wire grid, the mesh size must be small compared to the wavelength of the energy in order to approximate a solid conductor. As such, the wire grid modeling the area where the electric field predictions are made is much denser than the grid modeling the rest of the LTO and return path as shown in Figure 8. The largest dimension in the dense mesh is approximately 0.35 meters. A wavelength of 0.35 meters corresponds to a frequency of over 850 MHz; this frequency, and several multiples thereafter, are well beyond the limits of this analysis. The largest dimension used in modeling the LTO/return path combination is 4.4 meters which is the half the length of the cylinder section of the return path. A wavelength of 4.4 meters corresponds to a frequency of approximately 68 MHz which is in the analysis bandwidth. Therefore, false resonances could appear as a result of inadequate geometric modeling of the return path.

#### GEMACS Program Modules

Three GEMACS program modules were used in the analysis. The first module, GEMINP, read the program file and geometry data. Next, the GEMMOM module was run to perform the MOM analysis. Finally, the GEMOUT module was run to output the computed fields. Instead, though, of running each module



individually, a VMS command file was set up and the analysis was submitted as a batch job. This allowed the entire process to be run with just one command.

#### GEMACS Output

The output file produced by GEMACS was obtained by printing out CYLINDER.OUT. A summary of the output file's contents is given below.

INPUT Module. The first thing in the output file is a history of the GEMINP module's actions. When the input module is run, the program file and geometry commands are scanned for syntax errors. If none are found, GEMACS then constructs an interaction matrix from the geometry data. Also, a listing of the geometry elements with the exact coordinates and connection information for each segment is generated.

MOM Module. In the MOM module, the first task accomplished is to set the analysis frequency. Next, the source segment is excited. The interaction matrix is then decomposed and any structure loading applied. Then, the MOM technique is used to solve for the segment currents. Finally, the segment currents are used to calculate electric fields at the points specified by the user.

OUTPUT Module. The primary purpose of the OUTPUT module was to output the electric field values calculated in the MOM module. If the user had wanted further information from this problem, execution could be started from this

module and the interaction matrix would not have to be resolved again.

This chapter presented the processes that took place in modeling a lightning strike on the LTO with GEMACS. First, the LTO was geometrically modeled as a wire grid with the GEMACS GIP. Then, the model was excited and wire segment currents were calculated using the MOM. Finally, electric fields were calculated at several places around the LTO. The next chapter compares the GEMACS field predictions to experimental results.

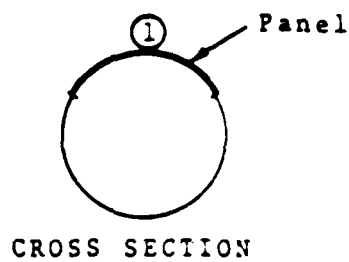
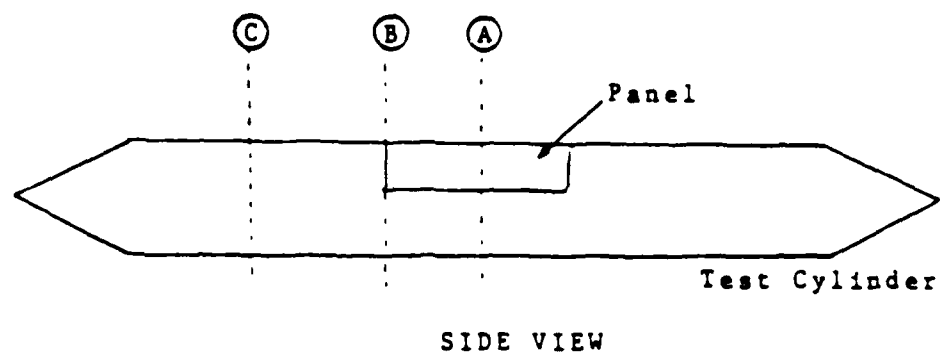
## V. Results

### Overview

The main purpose of this chapter is to present the results of the GEMACS analysis on the LTO and compare them to measured experimental data. This comparison is accomplished using GEMACS predicted LTO wire grid EM field transfer functions and LTO transfer functions produced experimentally in concurrent studies. In preparation for the discussion of the GEMACS and experimental data, some information on the experimental setup and procedure is given to understand why the GEMACS analysis and comparison were performed in the manner that they were.

### LTO Areas Analyzed

Field levels could be calculated by GEMACS at any position on the LTO model. However, in the experimental procedure, field measurements were taken only at the positions indicated in Figure 9. Only measurements taken at position A1 were used for this analysis because at that position, assuming a perfect conductor, the tangential electric fields should be approximately zero. An aluminum panel was placed in the aperture to approximate a perfect conductor. The only significant electric field should be in the transverse  $z$  direction and, as stated in Chapter II, should be related to the tangential magnetic field by the characteristic impedance. The geometry was entered into



A1  
B1  
C1

Figure 9. Sensor Locations

GEMACS such that all predictions were calculated in terms of x,y and z components to make the comparison comparison with measured data direct.

### Experimental Results

Figures 10 through 12 show the transfer functions obtained experimentally for the LTO/return path combination, LTO only and return path only. All the transfer functions show the same general characteristics of a smooth, flat response up to about 10 MHz and then periodic resonances afterwards.

It has been suggested that resonances in the transfer functions can be related to geometrical dimensions of the test object (10:6). At 10 MHz, the wavelength of the energy is 30 meters giving a half wavelength resonance of 15 meters which is closely approaching the long dimensions of the return path. As the frequency increases, the wavelengths get smaller and more resonances are found due to the smaller dimensions of the LTO. Distances such as LTO length and diameter, return path diameter, distance between LTO and return path, and the distances between the wires in the return path can all cause resonances.

### GEMACS Results

The GEMACS program predicted electric fields using the MOM to solve the interaction matrix generated for each configuration of the LTO. The LTO wire grids were composed

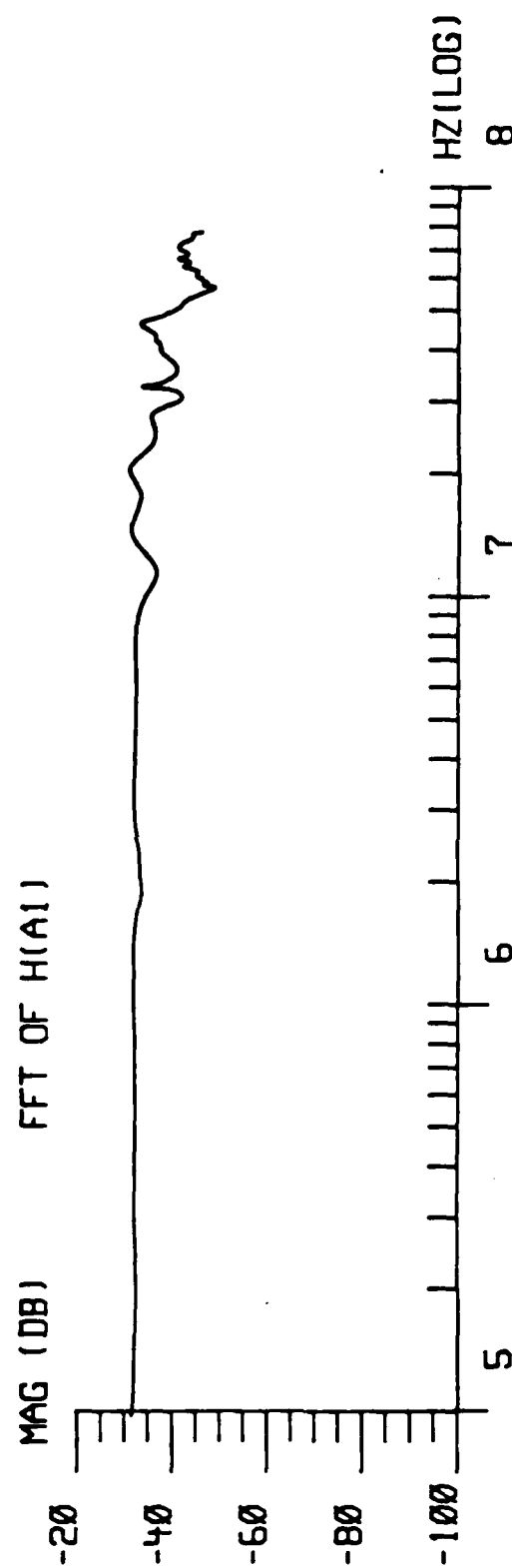


Figure 10. Experimental Transfer Function for  
LTO/Return Path

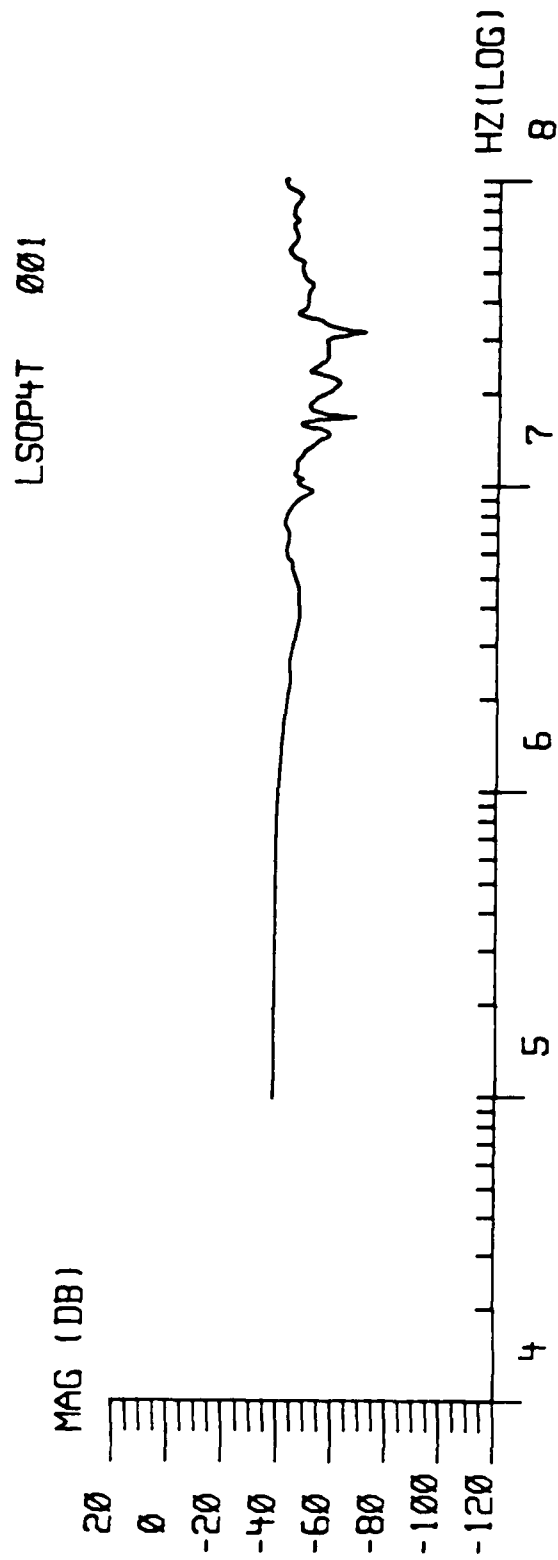


Figure 11. Experimental Transfer Function for LTO

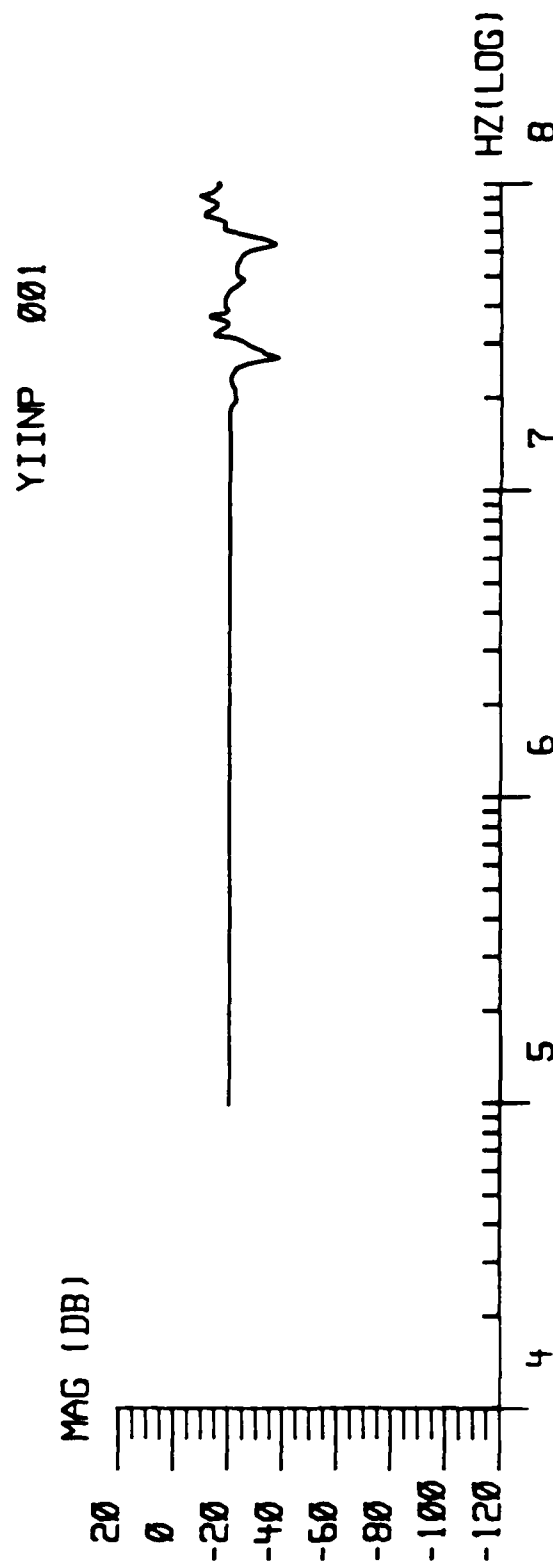


Figure 12. Experimental Transfer Function for Return Path



of various numbers of segments depending on the configuration being analyzed. All wire grids were terminated into an infinite ground plane located at  $z = 0$ . The analysis was performed at frequencies between 1 and 100 MHz.

Derivation of Transfer Functions. The predicted electric fields were used to derive LTO wire grid transfer functions which were then compared to experimentally obtained LTO transfer functions. The wire grid transfer functions were obtained by dividing the predicted electric field by the delta-gap electric field induced on the input segment at a specific frequency. Since the input electric field was always 1 V/m, as defined by the GEMACS voltage source excitation command, the magnitude of the electric field predicted at the sensor location was normalized and is plotted against frequency as the transfer function of the wire grid.

Resulting Transfer Functions. Figures 13 through 15 show the GEMACS predicted transfer functions obtained for the various configurations of the LTO. As in the experimental transfer functions, the response is smooth up to about 10 MHz and then resonances begin to occur. Geometrical aspects of the various LTO configurations are responsible for several of the resonances found in the transfer functions. All of the transfer functions have resonant spikes in the 25 - 30 MHz range which correspond to a second half-wavelength multiple of 10 - 12 meters which is

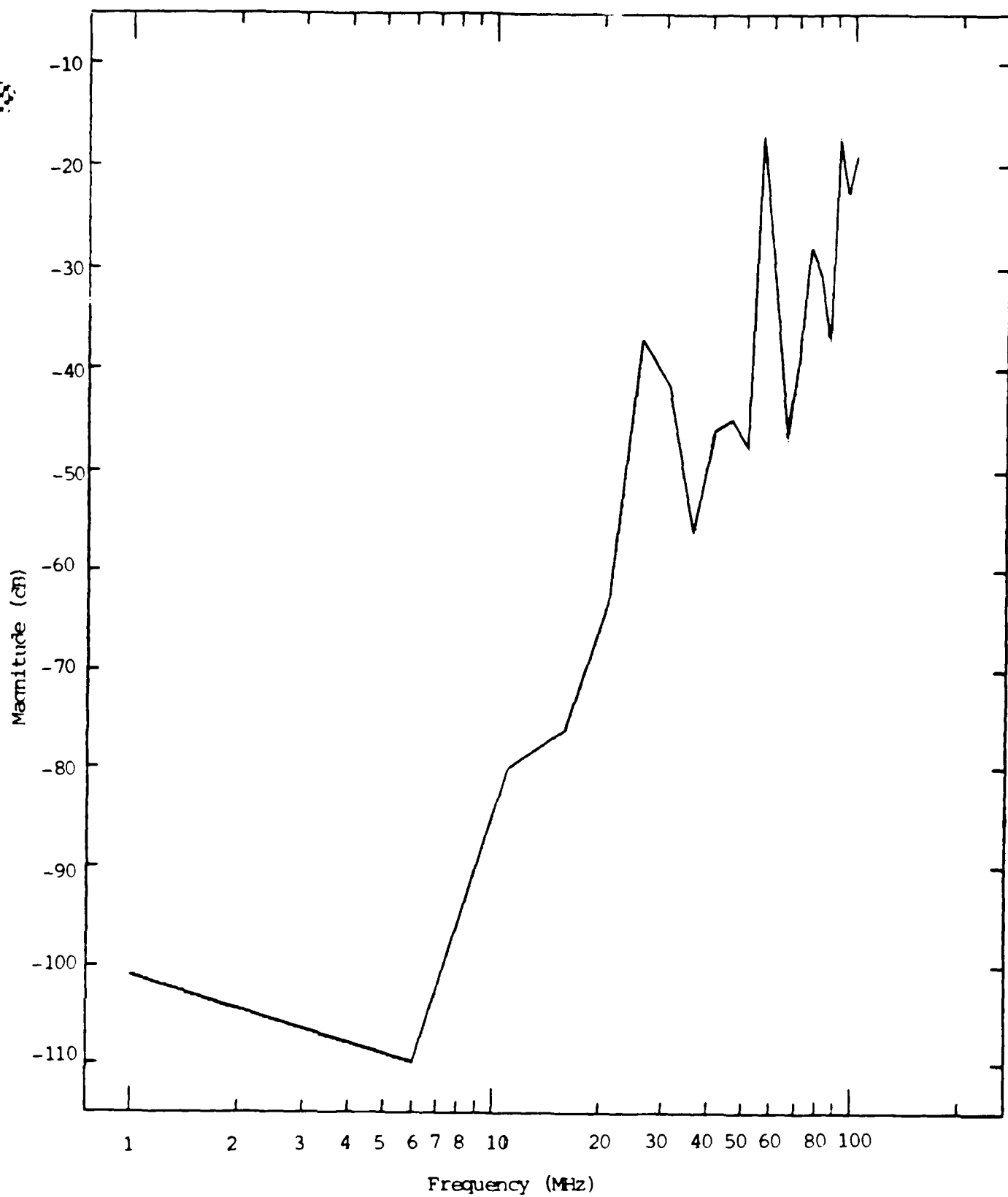


Figure 13. GEMACS Predicted Transfer Function for LTO/Return Path

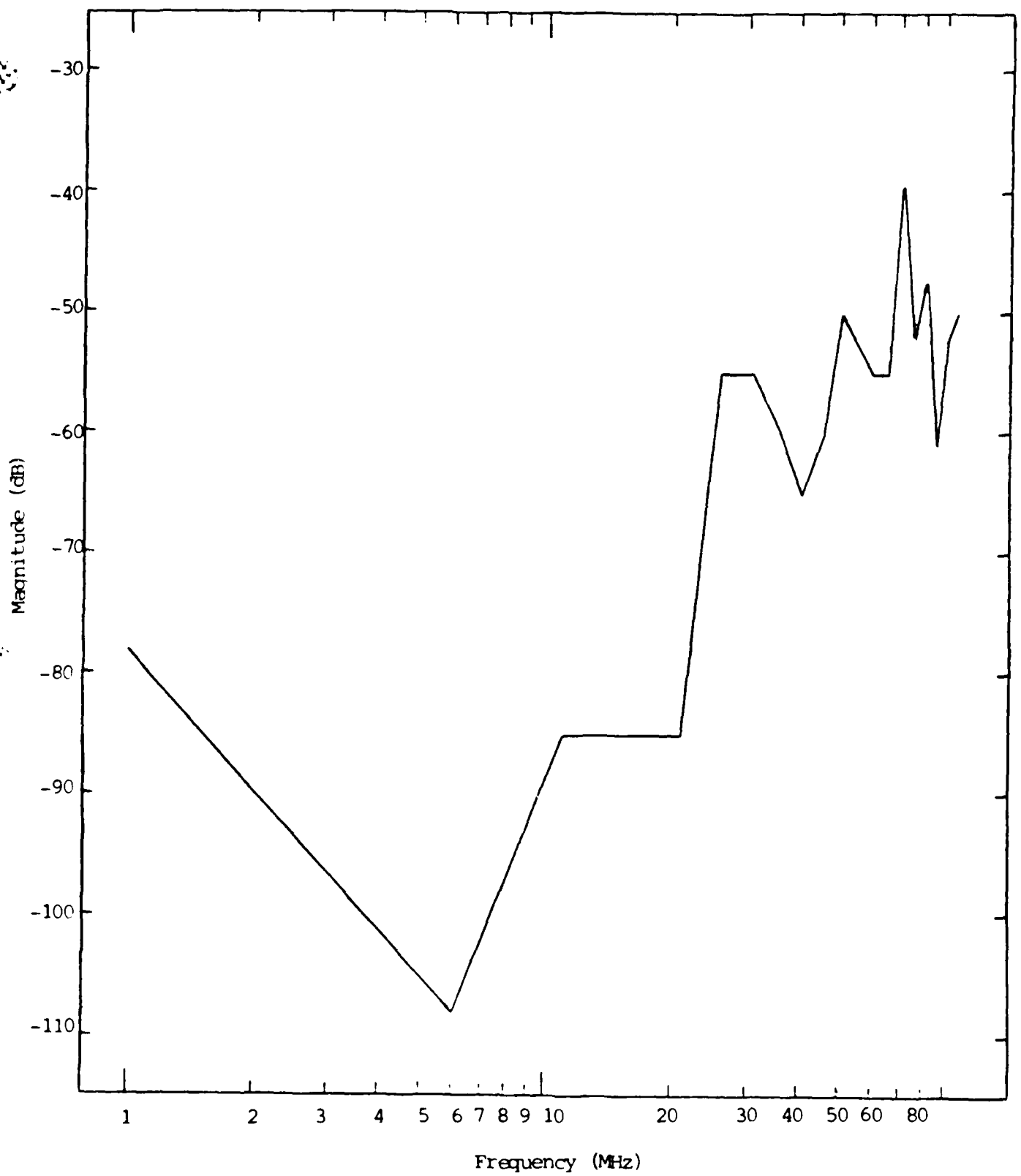


Figure 14. GEMACS Predicted Transfer Function for LTO

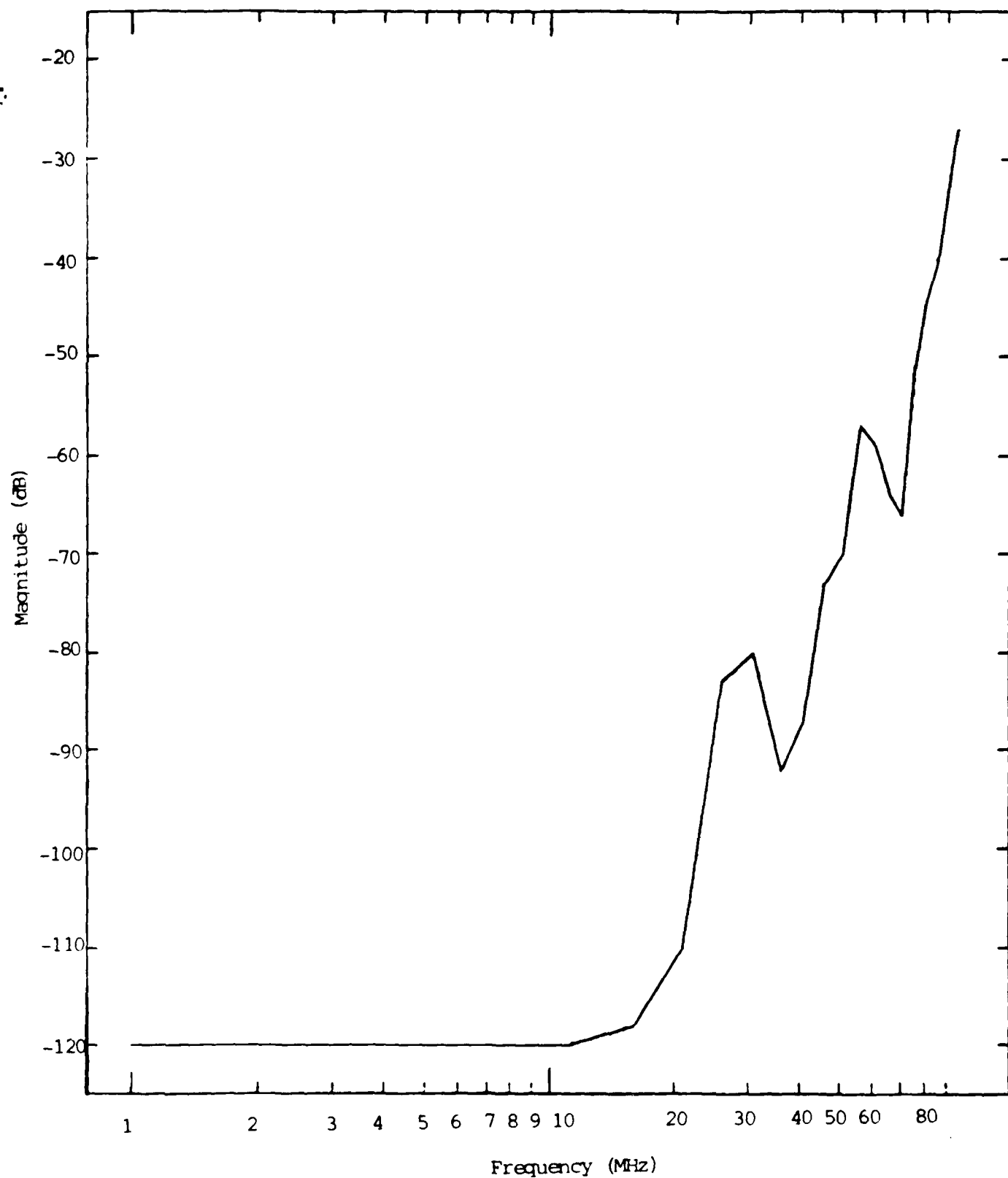


Figure 15. GEMACS Predicted Transfer Function for Return Path

very close to the length of the LTO. The two configurations with coaxial return paths exhibit resonances at approximately 55 MHz which corresponds to a half-wavelength of 2.7 meters; the approximate diameter of the return path. Other resonances are probably due to higher order half-wavelength resonances, mutual coupling between the LTO and the return path, and shorter connecting cables at the ends of the cylinder.

#### Comparison of GEMACS and Experimental Data

The transfer functions derived from GEMACS results were compared to the transfer functions obtained experimentally. Only the shapes of transfer functions and locations of resonances were compared because the magnitudes of the transfer functions, since they are linear solutions of Maxwell's equations, are directly proportional to the response at higher amplitudes.

The GEMACS and experimental predictions are shown together in Figures 16 through 18. The predicted LTO/return path combination compared quite well with the experimental results as shown in Figure 16. Both predicted and experimental results show resonances at approximately 30, 45, 55, 75 and 90 MHz. GEMACS, however, did not predict other smaller resonances seen in the experimental data. This is probably due to the fact that the GEMACS analysis was performed at discrete frequencies whereas the measured data was obtained over a continuous range of frequencies.

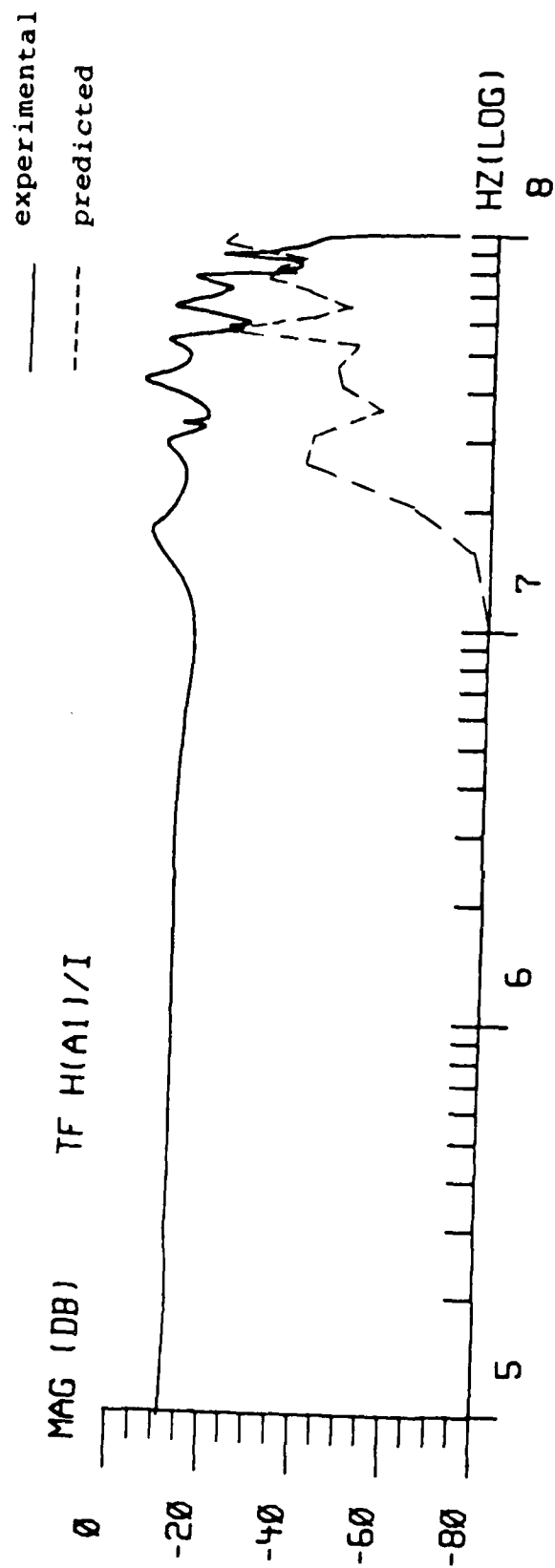


Figure 16. Comparison of LTO/Return Path Transfer Functions

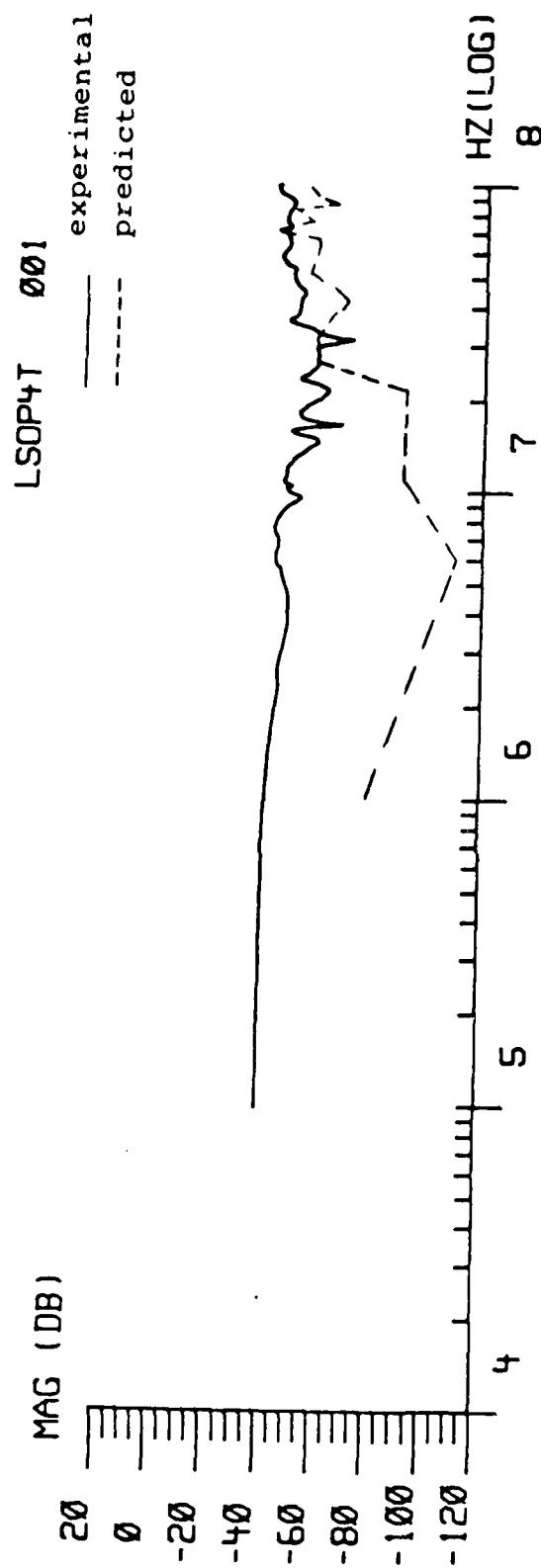


Figure 17. Comparison of LTO Transfer Functions

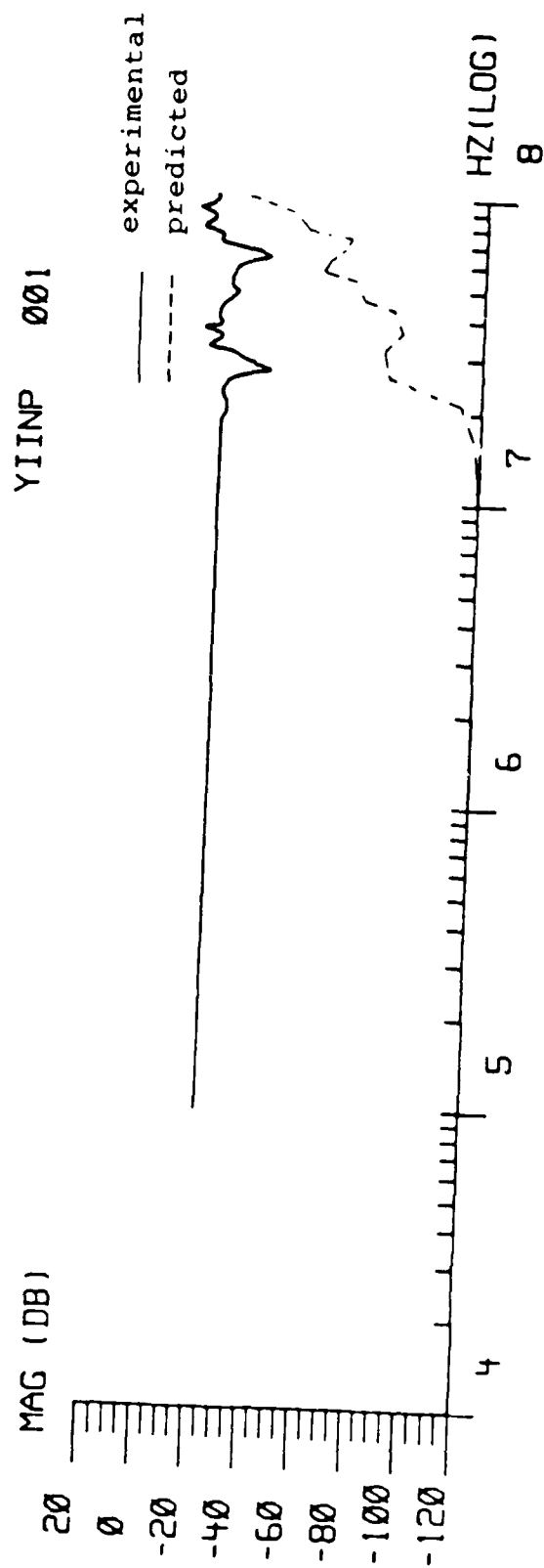


Figure 18. Comparison of Return Path Transfer Functions



Also, GEMACS did not predict the flat response seen at frequencies below 10 MHz. Several reasons could cause this discrepancy including the limited number of analysis frequencies in the 1 - 10 MHz range.

Figure 17 shows transfer functions for the LTO alone. Resonances predicted by GEMACS did not match as well as they did for the previous case. GEMACS predicted resonances at approximately 30, 50, 70, 80 and 90 MHz while experimental data shows resonances at 10, 20, 35 and 60 MHz. The shapes, however, of the two curves match well. As in the first case, GEMACS did not predict the low frequency response very accurately.

The GEMACS and experimental responses for the return path are shown in Figure 18. Both responses indicate resonances at 30 and 80 MHz. GEMACS does not predict the resonances at 40 and 90 MHz and again misses on the low frequency response.

### Summary of Results

Comparison between the GEMACS and measured data showed that GEMACS did a good job of predicting the general shape of the EM field characteristics over the analysis frequency range. A relatively flat response was predicted in the 1 - 10 MHz frequency range and the highly resonant features of the 10 - 100 MHz frequency range, due to the geometry of the LTO, showed up on both the GEMACS and measured data. On the other hand, GEMACS had trouble accurately predicting the

magnitudes of the measured data. This discrepancy could be attributed to the method used to excite the LTO. When the source segment was excited, a magnetic field was set up in a circular pattern around the wire. The source segment was connected to eight other segments which also generated magnetic fields. The interaction of these fields, called mutual coupling, can cause losses in the signal on the wires (11). Another cause could be the large mesh size used to model the return path. The return path was not modeled as densely as the LTO because GEMACS limits the number of user-defined points to 100. A large number of points were devoted to the LTO surface because it was thought that it was more important to accurately model the surface of the LTO than the return path since that is where the electric field measurements would be taken. Another factor that could contribute to the differences is the modeling of the LTO with perfectly conducting wire segments. If the segments had been electrically loaded, the transfer functions would have been a more realistic representation of the energy/structure interaction.

Overall, bearing in mind the limitations of excitation and geometric modeling presented here, GEMACS can adequately predict the shape of the EM field characteristics induced by injected currents as a function of frequency. The GEMACS analysis and results are summarized and recommendations for future research are made in the final chapter.

## VI. Summary and Conclusions

### Overview

This thesis was an attempt to find a model that can predict the electromagnetic (EM) fields produced when lightning strikes an aircraft. In a broader sense, it was a continuation of an ongoing process to determine the effects of lightning induced electromagnetic fields on aircraft and aircraft systems. The discovery of a model that can accurately predict these EM fields could provide the Air Force a method of safely and economically testing how different aircraft respond to the lightning threat.

### Objectives Revisited

The major objectives for this study have been successfully completed. Wire grid models of the LTO/return path combination and its constituent components were constructed. The experimental test configuration was studied to determine what differences there were between it and the modeling process. GEMACS analyses were performed on the wire grid models using the Method of Moments (MOM) to predict the electric fields around the LTO. It was found that magnetic field predictions were directly related to the electric field predictions due to the TEM nature of the test set configuration. Comparisons were made between the GEMACS predictions and measured data to assess the accuracy of the modeling technique.

### Summary of Conclusions

Comparison between the GEMACS and measured data showed that GEMACS did a good job of predicting the general shapes of the EM field characteristics. GEMACS predicted several resonances that could be attributed to LTO and return path geometries. GEMACS, however, did not predict magnitudes of the fields seen in the measured results. This difference was attributed to mutual coupling at the excitation segment. The limited number of analysis frequencies and inadequate geometric modeling due to the limited number of points allowed by GEMACS could also have affected the predicted results. If more points were allowed, the return path could have been modeled more accurately. Also, incorporating electrical loading of the segments into the model may have increased the correlation of the predicted and actual results.

### Recommendations

Several recommendations for future research can be made pursuant to the results of this study:

1. The version of GEMACS used in this study (3.15) is not the latest. Rome Air Development Center (RADC) has now completed GEMACS Version 4 and AFIT was in the process of ordering it when this study was being performed. Also, RADC has developed a version of GEMACS for use on IBM PC type computers. One recommendation would be to exercise the new

GEMACS programs to determine if the differences between the predicted and measured data noted in this study were due to problems with the older version.

2. Find a way to excite the source segment such that the magnitude of the signal on the connecting segments is not degraded due to mutual coupling between segments.

3. Analysis at even more frequencies than in this study would better reveal the capabilities of this version of GEMACS to predict EM fields.

4. Determine how to optimally distribute points when modeling a structure using a subsectional method such as MOM.

5. Use the Magnetic Field Integral Equation (MFIE) to first model the LTO as a series of patches and then solve for the surface currents and predict EM fields.

### Conclusion

This thesis showed that GEMACS can be a useful and economical tool in modeling the lightning/aircraft interaction event. The ability of GEMACS to predict the shape of the EM field characteristic around the LTO indicates that it can aid in determining how to protect aircraft systems from lightning damage. The LTO is also a useful item in studying lightning effects. It provides an aircraft like testbed with which engineers can perform lightning research without using aircraft from the Air Force inventory.

## Appendix

### GEMACS Files

#### Overview

The purpose of this appendix is to explain the specifics of building the GEMACS geometry input file, GEMACS program file and VMS command file.

#### Geometric Modeling

The first step in the modeling process is to obtain a drawing of the object to be modeled including its various dimensions. Next, a wire grid model of the object is made from the drawing. The GEMACS Engineering and User manuals give guidelines to follow when dividing the drawing into segments. Also, Tomko developed a step-by-step approach to constructing a wire grid model in his thesis (21:99-113).

Describing the wire grid model to the GEMACS program is the next step. This is done through the GEMACS Geometry Input Processor (GIP). For a strict wire grid model the only GIP commands needed are:

PT n x y z - defines a point in the Cartesian coordinate system. For example, PT 1 2. 3.5 -4. places a point at location  $(x,y,z)=(2,3.5,-4)$ .

CP n m s t r - means to connect PT n to PT m with s segments between the points. All the segments have a user defined tag of t and a radius defined by entry r in the radius table. It was found that the tag option was very useful because GEMACS' method of numbering segments was not entirely obvious.

RA r1 r2 r3 ... r10 - defines the radius table. For example RA .2 .03 4.5 means that all segments with radius entry 1 have radius .2 meters, all segments with radius entry 2 have radius .03 meters and so on. The version of GEMACS used in this thesis allowed for only ten entries in the radius table.

Figure 19 shows the GIP commands and data for the LTO wire grid model.

#### GEMACS Program File

The program file is written in GEMACS command language and allows the user to perform operations on the geometry data. "The GEMACS command language is a free-field, keyword oriented input stream" (10:15). All the commands are read by the input processor to check for errors prior to execution. The only restriction on symbolic names provided by the user is that they have five characters or less, the first character has to be alphabetic and the rest alphanumeric. Also, the following reserved keywords can not be used as symbolic names:

```

PT 1 0 0 2
PT 2 -0 33 0 2
$
PT 3 -1 034 0 2 501
PT 4 -1 034 -0 425 2 265
PT 5 -1 034 -0 501 2
PT 6 -1 034 -0 354 1 644
PT 7 -1 034 0 1 499
PT 8 -1 034 0 354 1 644
PT 9 -1 034 0 501 2
PT 10 -1 034 0 425 2 265
PT 11 -4 692 0 2 501
PT 12 -4 692 -0 166 2 473
PT 13 -4 692 -0 313 2 391
PT 14 -4 692 -0 425 2 265
PT 15 -4 692 -0 501 2
PT 16 -4 692 -0 354 1 644
PT 17 -4 692 0 1 499
PT 18 -4 692 0 354 1 644
PT 19 -4 692 0 501 2
PT 20 -4 692 0 425 2 265
PT 21 -4 692 0 313 2 391
PT 22 -4 692 0 166 2 473
PT 23 -4 9968 0 2 501
PT 24 -4 9968 -0 166 2 473
PT 25 -4 9968 -0 313 2 391
PT 26 -4 9968 -0 425 2 265
PT 27 -4 9968 0 425 2 265
PT 28 -4 9968 0 313 2 391
PT 29 -4 9968 0 166 2 473
PT 30 -5 3016 0 2 501
PT 31 -5 3016 -0 166 2 473
PT 32 -5 3016 -0 313 2 391
PT 33 -5 3016 -0 425 2 265
PT 34 -5 3016 0 425 2 265
PT 35 -5 3016 0 313 2 391
PT 36 -5 3016 0 166 2 473
PT 37 -5 6064 0 2 501
PT 38 -5 6064 -0 166 2 473
PT 39 -5 6064 -0 313 2 391
PT 40 -5 6064 -0 425 2 265
PT 41 -5 6064 0 425 2 265
PT 42 -5 6064 0 313 2 391
PT 43 -5 6064 0 166 2 473
PT 44 -5 9112 0 2 501
PT 45 -5 9112 -0 166 2 473
PT 46 -5 9112 -0 313 2 391
PT 47 -5 9112 -0 425 2 265
PT 48 -5 9112 0 425 2 265
PT 49 -5 9112 0 313 2 391
PT 50 -5 9112 0 166 2 473
PT 51 -6 216 0 2 501
PT 52 -6 216 -0 166 2 473
PT 53 -6 216 -0 313 2 391
PT 54 -6 216 -0 425 2 265
PT 55 -6 216 -0 501 2
PT 56 -6 216 -0 354 1 644
PT 57 -6 216 0 1 499
PT 58 -6 216 0 354 1 644
PT 59 -6 216 0 501 2
PT 60 -6 216 0 425 2 265
PT 61 -6 216 0 313 2 391
PT 62 -6 216 0 166 2 473
PT 63 -6 874 0 2 501
PT 64 -6 874 -0 425 2 265
PT 65 -6 874 -0 501 2
PT 66 -6 874 -0 354 1 644
PT 67 -6 874 0 1 499
PT 68 -6 874 0 354 1 644
PT 69 -6 874 0 501 2
PT 70 -6 874 0 425 2 265
PT 71 -10 578 0 2
PT 72 -10 908 0 2
PT 73 -9 874 0 3 143
PT 74 -9 874 -0 808 2 808
PT 75 -9 874 -1 143 2
PT 76 -9 874 -0 808 1 192
PT 77 -9 874 0 857
PT 78 -9 874 0 808 1 192
PT 79 -9 874 1 143 2
PT 80 -9 874 0 808 2 808
PT 81 -5 454 0 3 143
PT 82 -5 454 -0 808 2 808
PT 83 -5 454 -1 143 2
PT 84 -5 454 -0 808 1 192
PT 85 -5 454 0 857
PT 86 -5 454 0 808 1 192
PT 87 -5 454 1 143 2
PT 88 -5 454 0 808 2 808
PT 89 -1 034 0 3 143
PT 90 -1 034 -0 808 2 808
PT 91 -1 034 -1 143 2
PT 92 -1 034 -0 808 1 192
PT 93 -1 034 0 857
PT 94 -1 034 0 808 1 192
PT 95 -1 034 1 143 2
PT 96 -1 034 0 808 2 808
PT 97 2 0 2
PT 98 3 0 2
PT 99 3 0 0
RA 0 0405 0 079 0 0891 0 0505
RA 0 0703 0 168 0 0308
RA 0 160 0 202 0 214
CP 1 2 1 0 1
$
CP 2 3 2 1 2
CP 2 4 2 2 2
CP 2 5 2 3 2
CP 2 6 2 4 2
CP 2 7 2 5 2
CP 2 8 2 6 2
CP 2 9 2 7 2
CP 2 10 2 8 2
$
CP 3 4 1 9 3
CP 4 5 1 10 4
CP 5 6 1 11 5
CP 6 7 1 12 5
CP 7 8 1 13 5
CP 8 9 1 14 5
CP 9 10 1 15 4
CP 10 3 1 16 3
$
CP 3 11 4 17 6
CP 4 14 4 18 6
CP 5 15 4 19 6
CP 6 16 4 20 6
CP 7 17 4 21 6
CP 8 18 4 22 6
CP 9 19 4 23 6
CP 10 20 4 24 6
$
CP 11 12 1 25 7
CP 12 13 1 26 7
CP 13 14 1 27 5
CP 14 15 1 28 4
CP 15 16 1 29 5
CP 16 17 1 30 5
CP 17 18 1 31 5
CP 18 19 1 32 5
CP 19 20 1 33 4
CP 20 21 1 34 5
CP 21 22 1 35 7
CP 22 11 1 36 7
$
CP 11 23 1 37 4
CP 12 24 1 38 4
CP 13 25 1 39 4
CP 14 26 1 40 4
CP 15 33 1 41 3
CP 16 36 1 42 3
CP 17 37 1 43 3
CP 18 38 1 44 3
CP 19 39 1 45 3
CP 20 27 1 46 4
CP 21 28 1 47 4
CP 22 29 1 48 4
$
CP 26 25 1 49 5
CP 25 24 1 50 7
CP 24 23 1 51 7
CP 23 29 1 52 7
CP 29 28 1 53 7
CP 28 27 1 54 5
$
CP 23 30 1 55 4
CP 24 31 1 56 4
CP 25 32 1 57 4
CP 26 33 1 58 4
CP 27 34 1 59 4
CP 28 35 1 60 4
CP 29 36 1 61 4
$
CP 33 32 1 62 5
CP 32 31 1 63 7
CP 31 30 1 64 7
CP 30 36 1 65 7
CP 36 35 1 66 7
CP 35 34 1 67 5
$
CP 30 37 1 68 4
CP 31 38 1 69 4
CP 32 39 1 70 4
CP 33 40 1 71 4
CP 34 41 1 72 4
CP 35 42 1 73 4
CP 36 43 1 74 4
$
CP 40 39 1 75 5
CP 39 38 1 76 7
CP 38 37 1 77 7
CP 37 43 1 78 7
CP 43 42 1 79 7
CP 42 41 1 80 5
$
CP 37 44 1 81 4
CP 38 45 1 82 4
CP 39 46 1 83 4
CP 40 47 1 84 4
CP 41 48 1 85 4
CP 42 49 1 86 4
CP 43 50 1 87 4
$
CP 47 46 1 88 5
CP 46 45 1 89 7
CP 45 44 1 90 7
CP 44 50 1 91 7
CP 50 49 1 92 7
CP 49 48 1 93 5
$
CP 44 51 1 94 4
CP 45 52 1 95 4
CP 46 53 1 96 4
CP 47 54 1 97 4
CP 48 60 1 98 4
CP 49 61 1 99 4
CP 50 62 1 100 4
$
CP 51 52 1 101 7
CP 52 53 1 102 7
CP 53 54 1 103 5
CP 54 55 1 104 4
CP 55 56 1 105 5
CP 56 57 1 106 5
CP 57 58 1 107 5
CP 58 59 1 108 5
CP 59 60 1 109 4
CP 60 61 1 110 5
CP 61 62 1 111 7
CP 62 51 1 112 7
$
CP 51 63 1 113 6
CP 54 64 1 114 6
CP 55 65 1 115 6
CP 56 66 1 116 6
CP 57 67 1 117 6
CP 58 68 1 118 5
CP 59 69 1 119 6
CP 60 70 1 120 5
$
CP 63 64 1 121 3
CP 64 65 1 122 4
CP 65 66 1 123 5
CP 66 67 1 124 5
CP 67 68 1 125 5
CP 68 69 1 126 5
CP 69 70 1 127 4
CP 70 63 1 128 3
$
CP 63 71 2 129 2
CP 64 71 2 130 2
CP 65 71 2 131 2
CP 66 71 2 132 2
CP 67 71 2 133 2
CP 68 71 2 134 2
CP 69 71 2 135 2
CP 70 71 2 136 2
$
CP 71 72 1 137 1
$
CP 72 73 3 138 6
CP 72 74 3 139 6
CP 72 75 3 140 6
CP 72 76 3 141 6
CP 72 77 3 142 6
CP 72 78 3 143 6
CP 72 79 3 144 6
CP 72 80 3 145 6
$
CP 73 74 1 146 8
CP 74 75 1 147 8
CP 75 76 1 148 8
CP 76 77 1 149 8
CP 77 78 1 150 8
CP 78 79 1 151 8
CP 79 80 1 152 8
CP 80 73 1 153 8
$
CP 73 81 4 154 9
CP 74 82 4 155 9
CP 75 83 4 156 9
CP 76 84 4 157 9
CP 77 85 4 158 9
CP 78 86 4 159 9
CP 79 87 4 160 9
CP 80 88 4 161 9
$
CP 81 82 1 162 8
CP 82 83 1 163 8
CP 83 84 1 164 8
CP 84 85 1 165 8
CP 85 86 1 166 8
CP 86 87 1 167 8
CP 87 88 1 168 8
CP 88 81 1 169 8
$
CP 81 89 4 170 9
CP 82 90 4 171 9
CP 83 91 4 172 9
CP 84 92 4 173 9
CP 85 93 4 174 9
CP 86 94 4 175 9
CP 87 95 4 176 9
CP 88 96 4 177 9
$
CP 89 90 1 178 8
CP 90 91 1 179 8
CP 91 92 1 180 8
CP 92 93 1 181 8
CP 93 94 1 182 8
CP 94 95 1 183 8
CP 95 96 1 184 8
CP 96 89 1 185 8
$
CP 89 97 2 186 10
CP 90 97 2 187 10
CP 91 97 2 188 10
CP 92 97 2 189 10
CP 93 97 2 190 10
CP 94 97 2 191 10
CP 95 97 2 192 10
CP 96 97 2 193 10
$
CP 97 98 1 194 6
$
CP 98 99 1 195 10
END

```

Figure 19. GIP Commands and Data for LTO



A	C	D	N	O	R	V	X	Y	Z
CD	CR	CS	CW	CY	C1	C2	DC	DM	DP
DR	DT	DW	DX	DY	DZ	EC	ED	EI	ER
ES	EU	IS	LU	MM	NP	NR	ON	PC	PD
PL	PR	P1	P2	RC	RD	RR	R1	R2	SC
SW	T1	T2	VS	X1	X2	Y1	Y2	Z1	Z2
ABS	CDP	ECC	END	FRQ	GTD	ILP	INV	IRE	LUD
OFF	PDR	PHI	PRE	RDP	SEQ	SET	ASRC	AXIS	BAND
BCRE	BNDW	BSUB	CHPT	CLPE	CNVG	COND	EFLD	EPSR	ESRC
EXPD	FILE	GMDT	LGLG	LGLN	LGPL	LNLG	LNLN	LNPL	LOOP
MODL	MXIT	NFIL	OTPT	PLOT	PRLC	PSIN	READ	REDU	REFL
REPL	RSTT	SCDP	SEGS	SETI	SIZE	SNCS	SRDP	SRLC	SYMD
TAGS	TIME	TRSP	TYPE	VSRC	WIPO	ZCDS	ZGEN	ZIMP	ZLDS
ZMAT	CONJG	CPINC	CPNUM	DEBUG	INPUT	LABEL	PARTN	PIVOT	PRINT
PULSE	PURGE	SOLVE	STATS	TANG1	TANG2	THETA	TRACE	VALUE	WRITE

An example of a program file is given below with explanations for each command:

1. NFIL=23 - sets the number of temporary files, used to store intermediate program data, to 23.
2. TIME=1000 - sets the maximum amount of CPU minutes that can be spent on this problem to 1000.
3. FRQ=1.0 - sets the analysis frequency to 1.0 megahertz.
4. SETI MM - sets the solution technique to MOM.
5. GMDT=CYL - designates the geometry data set "CYL".

6. LOOP 1,20 - causes commands between this statement and the LABEL 1 statement to be executed 20 times (i.e. for 20 frequencies).
7. VIN=VSRC(CYL), V=1.0, 0., SEGS=1 - induces a delta-gap voltage of magnitude 1 volt, phase 0 degrees on segment number 1 of CYL
8. ZGEN ZMAT=ZCYL GMDT=CYL COND=-1 - generates an interaction matrix on CYL, stores the decomposed matrix, ZMAT, in ZCYL. COND=-1 designates z=0 a ground plane.
9. SOLVE ZCYL\*I=VIN - solves for the segment currents using the MOM technique.
10. PURGE ZCYL, ZUPR, ZLWR - purges unnecessary files.
11. FLD=EFLD(I) X1=-5.454 DX=0. X2=-5.454 Y1=0. DY=0. Y2=0.  
Z1=2.51 DY=0. Z2=2.51  
calculates the electric field from the currents at x=-5.454, y=0. and z=2.51. The DX, DY and DZ terms designate the increment to be used if the electric field is desired at more than one point. X2, Y2 and Z2 designate the upper bounds on the ranges.
12. FRQ=FRQ+5. - increments to the next analysis frequency.
13. LABEL 1 - returns control to LOOP statement.
14. END - ends program execution.

#### GEMACS Program Modules

Three GEMACS program modules were used in the analysis. The first module, GEMINP, read the program file and geometry data. Next, the GEMMOM module was run to

perform the MOM analysis. Finally, the GEMOUT module was run to output the computed fields. Instead, though, of running each module individually, a VMS command file was set up and the analysis was submitted as a batch job. This allowed the entire process to be run with just one command.

The VMS command file, RUNCYL.COM, used to perform the analysis is shown below with explanations for each command:

\$ ASSIGN CYLINDER.GEM SYS\$INPUT - assigns CYLINDER.GEM as  
the input file.

\$ ASSIGN CYLINDER.OUT SYS\$OUTPUT - creates an output file  
CYLINDER.OUT.

\$ RUN GEMINP - executes the GEMACS input module.

\$ RUN GEMMOM - executes the GEMACS MOM module.

\$ RUN GEMOUT - executes the GEMACS output module.

\$ DEASSIGN SYS\$INPUT - releases CYLINDER.GEM from input file  
status.

\$ DEASSIGN SYS\$OUTPUT - releases CYLINDER.OUT from output  
file status.

All that was required to execute the entire process was inputting the command "SUBMIT RUNCYL.COM" at the VMS dollar sign prompt. This command submitted the process as a batch job and released the terminal to the user to perform other processes.

## Bibliography

1. Beavin, R., and M.P. Hebert. "Atmospheric Electricity Hazards Protection Program (AEHP) Demonstration," Proceedings of the 11th International Aerospace and Ground Conference on Lightning and Static Electricity. Paper No 24: 1-5. Dayton OH, June 24-26, 1986.
2. Bishop, J., and R. Evans. "Induced Transients in Simulated Lightning Testing of the Fly-by-Wire Jaguar Aircraft," Proceedings of the 8th International Aerospace and Ground Conference on Lightning and Static Electricity. Paper No 41: 1-14. Fort Worth TX, June 21-23, 1983 (AD-P002195).
3. Burrows, B.J.C. Designers' Guide to the Installation of Electrical Wiring and Equipment in Aircraft to Minimise Lightning Effects. Abingdon, Oxfordshire OX14 3DB, United Kingdom: UKAEA Culham Laboratory, January 1981.
4. Burrows, B.J.C. Electromagnetic Shielding Properties of Graphite Epoxy Panels to Lightning: Final Report, January 1980-September 1980. Contract N00421-79-C-0017. Abingdon, Oxfordshire OX14 3DB, United Kingdom: UKAEA Culham Laboratory, September 1980.
5. Coffey, E.L., and J.L. Hebert. "Implementation of GEMACS for Lightning Interactions Analysis," Proceedings of the 11th International Aerospace and Ground Conference on Lightning and Static Electricity. Paper No 42: 1-5. Dayton OH, June 24-26, 1986.
6. Collin, R.E. Field Theory of Guided Waves. New York: McGraw-Hill Book Company, 1960.
7. Dorf, R.C. Modern Control Systems (Third Edition). Reading, Massachusetts: Addison-Wesley Publishing Company, 1980.
8. DuBro, G.A. Atmospheric Electricity Interactions with Aircraft. Lecture Series. Advisory Group for Aerospace Research and Development. Neuilly-Sur-Seine, France, May 1980 (AD-A087976).

9. Hardwick, C.J., and V.P. Dunkley. "Simulated Lightning Current Tests on a Lynx Helicopter," Proceedings of the 11th International Aerospace and Ground Conference on Lightning and Static Electricity. Paper No 13: 1-9. Dayton OH, June 24-26, 1986.
10. Hebert, J.L., and J.S. Reazer. "Current Levels and Distributions on an Aircraft Ground Lightning Simulation Tests and In-Flight Lightning Attachments," Proceedings of the 11th International Aerospace and Ground Conference on Lightning and Static Electricity. Paper No 18: 1-21. Dayton OH, June 24-26, 1986.
11. Hebert, M.P. Program Manager, Atmospheric Electricity Hazards Program, Advanced Development Program. Personal Interviews. AFWAL/FIEA, Wright-Patterson AFB OH, February 1987-May 1987.
12. Kadlec, D.L. and E.L. Coffey. GEMACS User Manual, (Version 3). The BDM Corporation, RADC-TR-83-217, Volume I, September 1983 (AD-A137461).
13. Kadlec, D.L. and E.L. Coffey. GEMACS Engineering Manual (Version 3). The BDM Corporation, RADC-TR-83-217, Volume I, September 1983 (AD-137462).
14. Kraus, J.D. Electromagnetics (Third Edition). New York: McGraw-Hill, 1984.
15. Labaune, G. and others. "Experimental Study of the Interaction Between an Arc and an Electrically Floating Structure," Proceedings of the 11th International Aerospace and Ground Conference on Lightning and Static Electricity. Paper No 27: 1-9. Dayton OH, June 24-26, 1986.
16. McCormick, W., K.J. Maxwell, and R. Finch. Analytical and Experimental Validation of the Lightning Transient Analysis Technique: Final Report, March 1977-November 1977. Contract F-33615-75-D-0090. Dayton OH: Technology Incorporated, March 1978.
17. Moore, J. and R. Pizer. Moment Methods in Electromagnetics. Letchworth, Hertfordshire, England: Research Studies Press, 1984

18. O'Neal, James L. Analysis of Lightning Induced Magnetic Field Penetration Through Protective Metal Screens Using an Equivalent Dipole Moment Representation of an Array of Elliptic Apertures. Master's Thesis, AFIT/GE/ENG/86D-30. School of Electrical and Computer Engineering, Air Force Institute of Technology (AU), Wright-Patterson AFB OH, December 1986.
19. Perala, F.J. Eriksen, and T.H. Rudolph. Atmospheric Electricity Hazards Analytical Model Development and Application, Volume III: Electromagnetic Coupling Modeling of the Lightning/Aircraft Interaction Event: Final Report, August 1979-June 1981. Contract F-33615-79-C-3412. Denver CO: Electromagnetic Applications, Inc., August 1981 (AD-A114017).
20. Rustan, P.L. "A Review of Aerospace and Ground Lightning Threat Characteristics and Applications," Proceedings of the 11th International Aerospace and Ground Conference on Lightning and Static Electricity. Paper No 1: 1-8. Dayton OH, June 24-26, 1986.
21. Tomko, F.G. GEMACS Frequency Domain Analysis to Determine the Lightning Induced Electromagnetic Skin Current Distributions on Aircraft. Master's Thesis, AFIT/GE/ENG/86D-10. School of Electrical and Computer Engineering, Air Force Institute of Technology (AU), Wright-Patterson AFB OH, December 1986.
22. Uman, M.A. Lightning. New York: Dover Publications, Inc., 1969.
23. Williford, C.F. Comparison of Absorption and Radiation Boundary Conditions Using a Time-Domain Three-Dimensional Finite Difference Electromagnetic Computer Code. Master's Thesis, AFIT/GE/ENG/85D-53. School of Electrical and Computer Engineering, Air Force Institute of Technology (AU), Wright-Patterson AFB OH, December 1985.

## VITA

Captain David S. Mabee was born on 9 September 1961 in Birmingham, Alabama. He graduated from high school in Huntsville, Alabama, in 1979 and attended Auburn University, from which he received the degree of Bachelor of Electrical Engineering in August 1983. Upon graduation, he received a commission in the USAF through the ROTC program. He was employed by Dynetics Corporation, Huntsville, Alabama as an associate engineer until called to active duty in November 1983. He served as an electronic warfare engineer with the Air Force Electronic Warfare Center, Kelly AFB, Texas, until entering the School of Engineering, Air Force Institute of Technology, in June 1986.

Permanent address: 710 Mira Vista Dr.  
Huntsville, Alabama 35802

## REPORT DOCUMENTATION PAGE

Form Approved  
OMB No. 0704-0188

1a REPORT SECURITY CLASSIFICATION UNCLASSIFIED		2b DECLASSIFICATION/DOWNGRADING SCHEDULE	
2a SECURITY CLASSIFICATION AUTHORITY		3 ABSTRACT	
4 PERFORMING ORGANIZATION REPORT NUMBER ADP 1000 1000 1000		5 AUTHORING ORGANIZATION REPORT NUMBER	
6a NAME OF PERFORMING ORGANIZATION DEFENSE INTELLIGENCE AGENCY	6b OFFICE SYMBOL (if applicable)	7a NAME OF MONITORING ORGANIZATION	
6c ADDRESS (City, State, and ZIP Code) AID, Defense Intelligence Agency AID 1000 1000 1000		7b ADDRESS (City, State, and ZIP Code)	
8a NAME OF FUNDING SPONSORING ORGANIZATION DEFENSE INTELLIGENCE AGENCY	8b OFFICE SYMBOL (if applicable)	9 MONITORING ORGANIZATION REPORT NUMBER	
8c ADDRESS (City, State, and ZIP Code) AID, Defense Intelligence Agency AID 1000 1000 1000		10 DISTRIBUTION STATEMENTS	
11 ABSTRACT (Include Security Classification)		12 PERSONAL AUTHOR	
13a TYPE OF REPORT Technical Report	13b DATE 1980	13c PERIODICITY Monthly	13d NUMBER OF PAGES 10
14 SUPPLEMENTARY NOTES			
15 DISTRIBUTION STATEMENTS		16 ABSTRACT	
17 ABSTRACT (Continue on separate page if necessary)			
18 NAME OF PERFORMING ORGANIZATION		19 NAME OF MONITORING ORGANIZATION	



The General Electromagnetic Model for the Analysis of Complex Systems (GEMACS) is used to model and perform a frequency domain analysis on a specially instrumented Air Force Lightning Test Object (LTO). The predicted results are compared to experimental data to evaluate GEMACS's ability to predict electromagnetic (EM) fields around the LTO. A previous elementary GEMACS study modeled an airplane and compared the results to lightning data collected in flight. Limitations of that effort included geometric modeling where some parts of the airplane were modeled more accurately than others and limited analysis bandwidth. The small bandwidth used in that GEMACS analysis made comparisons with the in-flight data difficult because the in-flight data had a much larger bandwidth. The present study analytically models the LTO most accurately at the places where the field predictions are made and uses a larger analysis bandwidth of 1-100 MHz. This study provides an initial baseline case on how accurately GEMACS predicts lightning induced EM fields, and further validation that frequency domain code can be an economical method by which lightning's interaction with aircraft can be predicted.

END

FILMED

MARCH, 19 88

DTIC